NORWEGIAN JOURNAL OF GEOLOGY Vol XX Nr. XX
https://dx.doi.org/10.17850/njg002

Geological Society of Norway

Fluid flow properties of the Wilhelmøya Subgroup, a potential unconventional CO_2 storage unit in central Spitsbergen

Mark Joseph Mulrooney[1,2], Leif Larsen[3], Jeroen Van Stappen[4], Bjarte Rismyhr[1,5], Kim Senger[1], Alvar Braathen[2], Snorre Olaussen[1], Mai Britt E. Mørk[6], Kei Ogata[7] & Veerle Cnudde[4]

[1]*Department of Arctic Geology, University Centre in Svalbard, P.O. Box 156, 9171 Longyearbyen, Norway.*
[2]*Department of Geosciences, University of Oslo, P.O. Box 1047, Blindern, 0316 Oslo, Norway.*
[3]*Department of Petroleum Engineering, University in Stavanger, P.O. Box 8600, Forus, 4036 Stavanger, Norway.*
[4]*Department of Geology, PProGRess-UGCT, Ghent University, Krijgslaan 281/S8, B–9000, Belgium*
[5]*Department of Earth Science, University of Bergen, P.O. Box 7803, N–5020 Bergen, Norway.*
[6]*Department of Geoscience and Petroleum, Norwegian University of Science and Technology, N–7491 Trondheim, Norway.*
[7]*Faculty of Earth and Life Sciences, Geology and Geochemistry cluster, VU Amsterdam, De Boelelaan 1085–1087, 1081 HV Amsterdam, Netherlands.*

E-mail corresponding author (Mark Joseph Mulrooney): mark.mulrooney@geo.uio.no

The Upper Triassic to Middle Jurassic Wilhelmøya Subgroup forms one of the more suitable reservoir units on the Norwegian Arctic archipelago of Svalbard. The target siliciclastic storage unit, which is encountered at approx. 670 m depth at the potential injection site in Adventdalen, central Spitsbergen, is a severely under-pressured (at least 35 bar), tight and compartmentalised reservoir with significant contribution of natural fractures to permeability. In this contribution, we characterise the 15–24 m-thick Wilhelmøya Subgroup storage unit using both borehole and outcrop data and present water-injection test results that indicate the presence of fluid-flow barriers and the generation of new, and propagation of pre-existing natural fractures during injection. Whole core samples from drillcores and outcrops were sampled for pore network characterisation and analysed using high-resolution X-ray computed tomography (Micro-CT). We demonstrate that heterogeneities such as structural discontinuities, igneous bodies and lateral facies variations, as examined in well core and equivalent outcrops, will strongly influence fluid flow in the target reservoir, both by steering and baffling fluid migration. Many of these heterogeneities are considered to be subseismic, and their detailed characterisation is important to predict subsurface CO_2 storage potential and optimise injection strategy.

Keywords: CCS, reservoir compartmentalisation, Spitsbergen

Received 10. October 2017 / Accepted 23. July 2018 / Published online 1. November 2018

Introduction

Longyearbyen is a small isolated community situated on the Arctic archipelago of Svalbard at 78° north (Fig. 1). The Longyearbyen CO_2 Lab was established in 2007 by the University Centre in Svalbard (UNIS) as a pilot-scale, onshore carbon capture and storage (CCS) study. The project aim was to assess the feasibility of capturing CO_2 emitted by the local, coal-fuelled power plant (approx. 60,000 tons of CO_2 emitted annually) and storing it in a saline aquifer underground.

Increase in anthropogenic emission of CO_2 into the Earth's atmosphere since the industrial revolution and its contribution to global climate change is unequivocal

Mulrooney, M.J., Larsen, L., Van Stappen, J., Rismyhr, B., Senger, K., Braathen, A., Olaussen, S., Mørk, M.B.E., Ogata, K. & Cnudde, V. 2018: Fluid flow properties of the Wilhelmøya Subgroup, a potential unconventional CO_2 storage unit in central Spitsbergen. *Norwegian Journal of Geology* 85-116. https://dx.doi.org/10.17850/njg002.

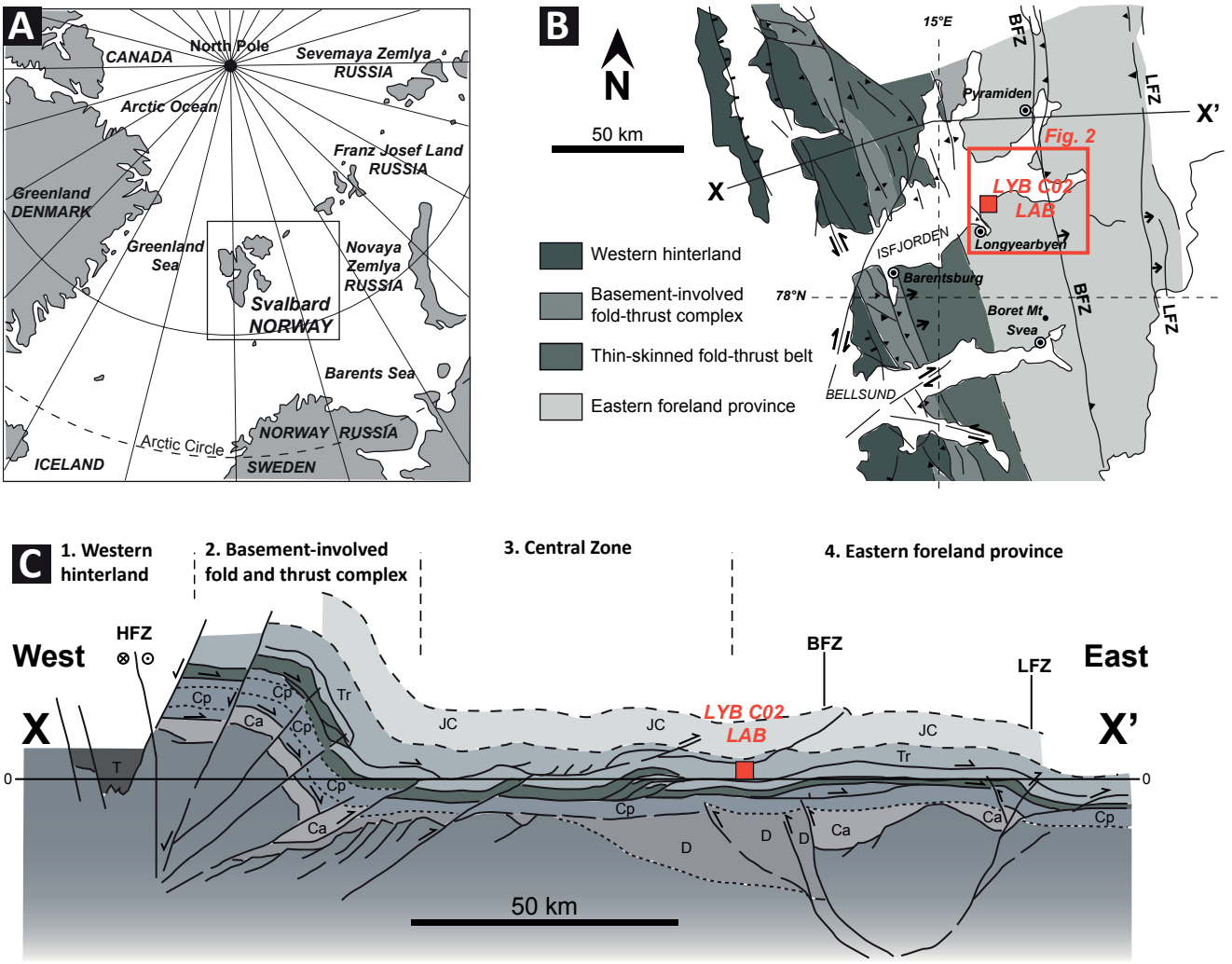

Figure 1. *Geographical and geological location of the Longyearbyen CO_2 Lab study site. (A) The CO_2 study is located on Spitsbergen, the largest island of the Svalbard archipelago, which is situated in the Arctic Ocean between 74° and 81°N and 15° and 35°E. (B) Simplified geological map of central Spitsbergen showing primary structural elements (modified from Ogata et al., 2012, 2014, after Dallmann et al., 2002); the Longyearbyen CO_2 Lab field study site is highlighted by a red square. (C) Generalised cross-section of Spitsbergen showing four structural zones of the Western Spitsbergen fold and thrust belt (WSFTB). Abbreviations: LYB CO_2 LAB – Longyearbyen CO_2 Laboratory, BFZ – Billefjorden Fault Zone, LFZ – Lomfjorden Fault Zone, HFZ - Hornsund Fault Zone, D – Devonian, Ca – Carboniferous, Cp – Permian, Tr – Triassic, JC – Jurassic–Cretaceous, T – Tertiary. Cross-section modified from Ogata et al. (2014), and based on Bergh et al. (1997).*

(IPCC, 2005; IEA, 2008). The '450 Scenario', aims for stabilisation of global atmospheric CO_2 at 450 ppm (the Copenhagen Accord). Carbon capture and storage (CCS) offers one such method of emission reduction (contributing up to 19%; Birol, 2010) where carbon is captured at point sources (e.g., coal-fuelled power plants), transported to suitable injection sites (e.g., by pipelines, ships or trucks) and injected into suitable subsurface storage formations, e.g., saline aquifers and depleted hydrocarbon fields (IPCC, 2005; Bachu, 2008; Benson & Cole, 2008).

The technology for injecting CO_2 into the subsurface is reasonably well understood and has been employed by the hydrocarbon industry since the 1980s for increasing oil recovery (Beliveau et al., 1993). CCS was tested and applied globally in a variety of geological and top-side settings within the past decade, with a varying degree of success. The technical feasibility of CCS is currently best illustrated by a handful of industrial-scale projects that have operated in recent years, e.g., Sleipner (Eiken et al., 2011), In Salah (Vasco et al., 2008), and the Weyburn field (White et al., 2004; Whittaker et al., 2004). Furthermore, pilot-scale projects in Japan (Xue et al., 2006), Ketzin in Germany (Förster et al., 2006), the Frio project in Texas (Daley et al., 2008; Doughty et al., 2008) and CarbFix in Iceland (Aradóttir et al., 2011) all confirm the feasibility of the storage part of CCS under various subsurface and top-side conditions.

The primary focuses of the Longyearbyen CO_2 Lab (Braathen et al., 2012) have been identification and appraisal of potential reservoir and caprock units. The best reservoir units have been identified as the

uppermost part of the Carnian to Norian De Geerdalen Formation (Isfjorden Member) and the Norian to Bathonian Wilhelmøya Subgroup, which are encountered at 672 to 970 metres depth at the potential injection site in Adventdalen (drill site 2; Fig. 2), 5 km southeast of the Longyearbyen power plant. The Wilhelmøya Subgroup has the best porosity and permeability but well tests confirm the presence of baffles to fluid flow (discussed herein).

The overlying shale- and claystone-dominated, late Bathonian to Hauterivian Agardhfjellet and Rurikfjellet formations were identified as a suitable caprock interval. The presence of a 100–150 m-thick permafrost zone at the drill site (Humlum et al., 2003; Johansen et al., 2003) is also expected to contribute locally as a complementary seal. The potential reservoir and caprock outcrop 15 km to the northeast of the planned injection site (Fig. 2) and, as such, no conventional structural trap is present (Bælum et al., 2012). Subhydrostatic pressure gradients in the reservoir (discussed herein), however, suggest that the reservoir is not in communication with the surface.

Analysis of outcrop and core data, along with water injection tests, have shown the reservoir to be tight, with low matrix permeability (<2 mD) and moderate porosity (up to 20%; Braathen et al., 2012; Farokhpoor et al., 2013, 2014; Mørk, 2013; Magnabosco et al., 2014; Senger et al., 2015a). The tight nature of the reservoir relates to deep burial that occurred during the development of the Palaeogene West Spitsbergen Fold-and-Thrust Belt (WSFTB; Bergh et al., 1997; Braathen et al., 1999). The reservoir is further complicated by the occurrence of Early Cretaceous igneous intrusions (Bælum et al., 2012; Corfu et al., 2013; Senger et al., 2014a), large-scale low-angle thrusts and subseismic high-angle extensional faults related to the WSFTB (Ogata et al., 2014; Mulrooney & Braathen, 2015). Despite these heterogeneities, water injection tests show an average flow capacity of 61 mD m^{-1} in the Wilhelmøya Subgroup (Larsen, 2010, 2012), which is envisaged to be primarily a function of matrix permeability, with the natural fracture network providing efficient fluid migration pathways from less to more promising reservoir zones. The underlying De Geerdalen Formation shows an average flow capacity of 45 mD m^{-1} in the lowermost part of the reservoir which is envisaged to be primarily a function of the natural fracture network (Larsen, 2010, 2012; Ogata et al., 2012, 2014).

Natural gas was encountered at several stratigraphic intervals during the drilling campaign (Senger et al., 2016; Huq et al., 2017; Ohm et al., 2017). Thermogenic gas and oil-stained sandstones were encountered in the De Geerdalen Formation (DH4; Fig. 2) and envisaged to have been generated in the Middle Triassic Botneheia Formation (Abay et al., 2017) located approx. 400 m below the maximum drilled depth. Thermogenic gas from a 650–703 m interval in well DH5R (Fig. 2) which spans the Wilhelmøya Subgroup and the lowermost part of the Agardhfjellet Formation Subgroup, was possibly sourced from the Agardhfjellet Formation (Ohm et al., in prep.), analogues to the Hekkingen Formation which is a prolific source rock in the SW Barents Sea.

As previously stated, a key finding from the pilot project is that subhydrostatic pressures are present in the storage formation interval. In addition, a slight overpressure is encountered in a shallow aquifer above the caprock (Braathen et al., 2012). Vertical pressure compartmentalisation (Braathen et al., 2012) illustrates the good sealing properties of the caprock, while lateral pressure compartmentalisation (Larsen, 2010, 2012) indicates the presence of baffles or seals to fluid flow. Moreover, this observation is supported by water injection tests in DH7A and interference monitoring in DH5R (UNIS CO_2 Lab AS, 2015) described herein. Communication between the two wells (situated 94 metres apart) during active injection was negligible, further supporting the presence of lateral flow barriers. The abnormal pressures encountered in the storage formation interval attest to a tight impermeable underburden consistent with the Bravaisberget Formation which forms the uppermost part of the Sassendalen Group.

This contribution presents evidence of fluid flow barriers affecting the target reservoir unit and details structural heterogeneities that may compartmentalise the potential storage unit.

Geological setting

The Svalbard archipelago is part of the emergent, uplifted northwest Barents shelf (Fig. 1), an otherwise submerged portion of Eurasian continental crust. The early development of the area is dominated by the Silurian–Devonian Scandian phase of the Caledonian orogeny (McKerrow et al., 2000), as well as earlier tectonic events, e.g., the Svecofennian and Timanian orogenies (Nironen, 1997; Ritzmann & Faleide, 2007; Faleide et al., 2008; Marello et al., 2010; Andresen et al., 2014). The oldest strata preserved on Svalbard comprise the Precambrian to Early Palaeozoic Hecla Hoek (Harland et al., 1966; Ohta, 1982) and form the region's metamorphic basement.

Following the Caledonian orogeny, uplifted areas were subject to subaerial erosion, with deposition of Old Red Sandstone taking place in supradetachment basins throughout the Devonian to Early Carboniferous (Faleide et al., 1993; Osmundsen et al., 1998; Braathen et al., 2000, 2018; Osmundsen & Andersen, 2001; Souche et al., 2012). This crustal-scale extension exploited north–south trending Caledonian lineaments and was followed

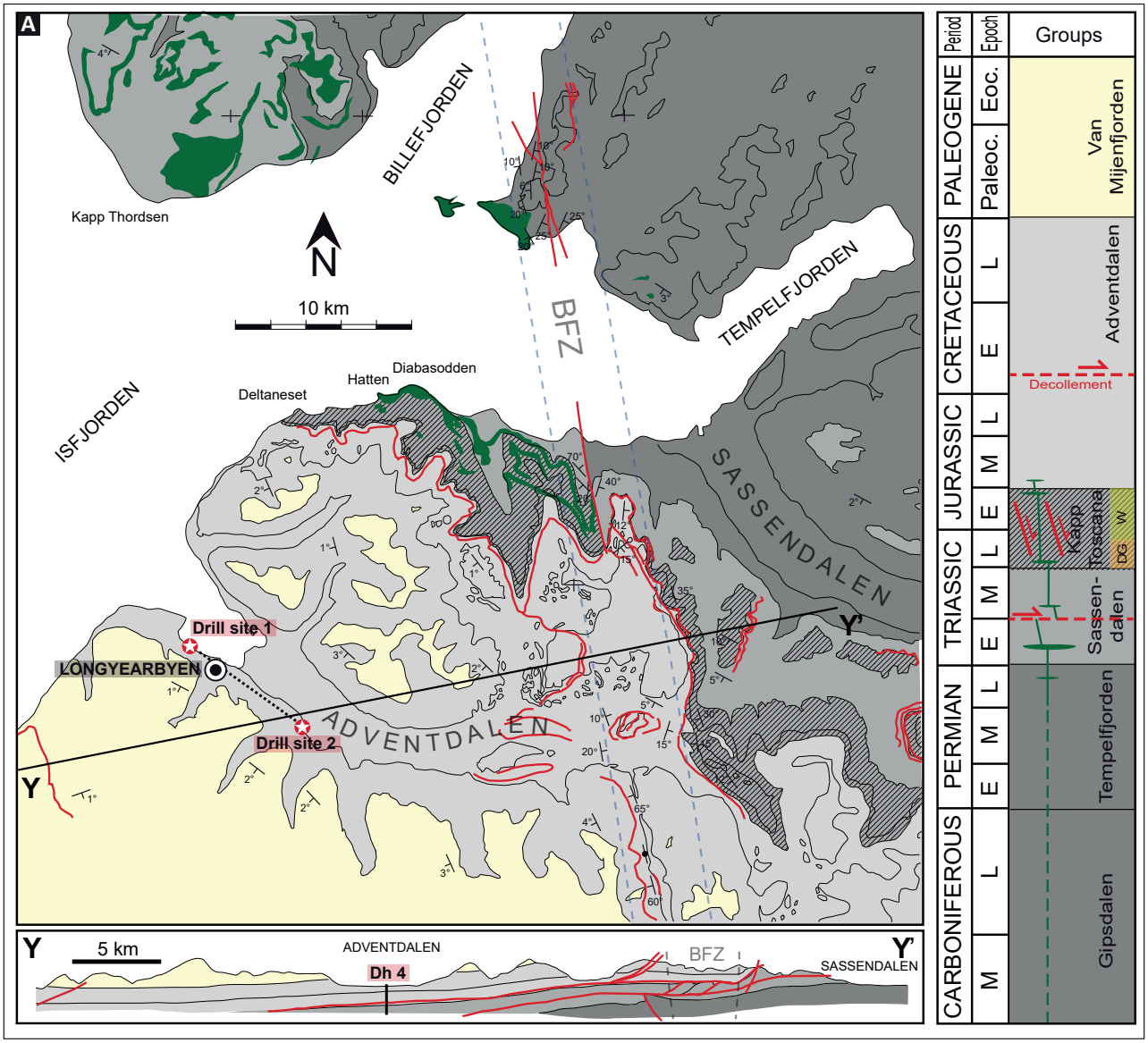

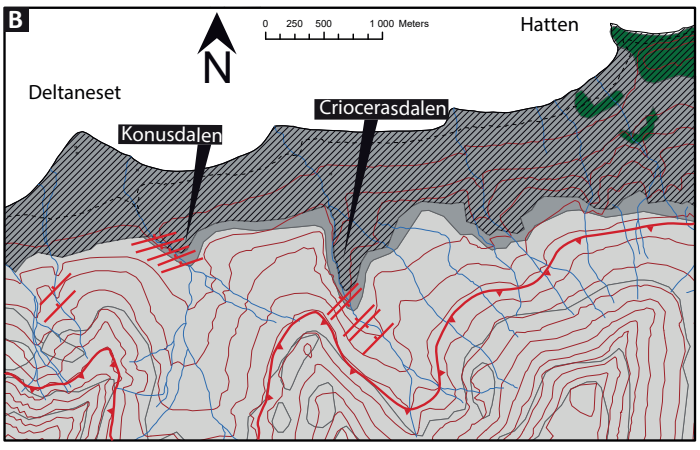

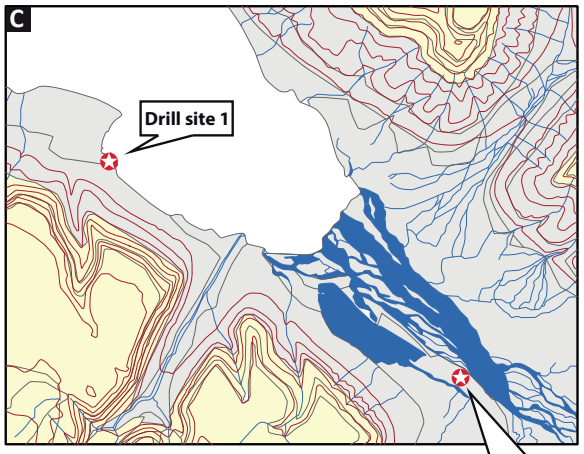

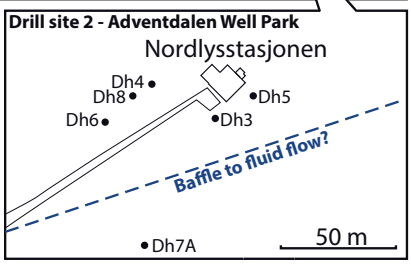

Igneous intrusions (L. Cretaceous)

Faults

Group boundary

BFZ Billefjorden Fault Zone

Bedding strike, dip direction and dip

45° Normal

Horizontal

Vertical

Figure 2. (A) Simplified geological map and cross-section of the Longyearbyen CO_2 Lab study site and surrounding area, modified from Major et al. (1992) and Ogata et al. (2012, 2014), based on Dallmann (1999). The inset simplified cross-section (Y–Y') and stratigraphic column show that the potential reservoir unit (within the Kapp Toscana Group) is sandwiched between two décollement surfaces related to the WSFTB. Abbreviations: DG – De Geerdalen Formation, W – Wilhelmøya Subgroup. The reservoir is also shown to be affected by small extensional faults (also associated with the WSFTB), and Late Cretaceous doleritic dykes and sills. (B) Simplified geological map of the Deltaneset to Hatten area, where the Longyearbyen CO_2 target reservoir crops out 15 km northeast of the proposed injection site (Drill site 2). Two valley sections, Konusdalen and Criocerasdalen, are highlighted, where faults and fractures have been investigated in both the reservoir and the caprock succession, respectively. (C) Simplified geological map of the Longyearbyen area showing the two drill sites. Inset: Map of the Aventdalen Well Park, which is the potential CO_2 injection site. Lab study site and surrounding area, modified from Major et al. (1992) and Ogata et al. (2012, 2014), based on Dallmann (1999). The inset simplified cross-section (Y–Y') and stratigraphic column show that the potential reservoir unit (within the Kapp Toscana Group) is sandwiched between two décollement surfaces related to the WSFTB. Abbreviations: DG – De Geerdalen Formation, W – Wilhelmøya Subgroup. The reservoir is also shown to be affected by small extensional faults (also associated with the WSFTB), and Late Cretaceous doleritic dykes and sills. (B) Simplified geological map of the Deltaneset to Hatten area, where the Longyearbyen (A) Simplified geological map and cross-section of the Longyearbyen CO_2.

by, or linked to, a phase of east–west crustal shortening during the latest Devonian to earliest Carboniferous Svalbardian–Ellesmerian deformation event (McCann, 2000; Piepjohn, 2000; Braathen et al., 2018). Narrow rift grabens, again reactivating Caledonian lineaments, formed in the Middle–Late Carboniferous, e.g., the Billefjorden Fault Zone (Braathen et al., 2011; Maher & Braathen, 2011) and were filled by a mixture of siliciclastic and evaporite deposits.

Extensional activity along lineaments slowed in the Late Carboniferous–Permian (Høy & Lundschien, 2011), and Permian carbonates and evaporites were deposited as part of a stable platform succession. Later Permian deposits record a shift from warm-water carbonates to cold-water, siliceous deposits (Steel & Worsley, 1984; Stemmerik & Håkansson, 1989; Stemmerik & Worsley, 1989; Nilsson et al., 1996; Worsley, 2008; Smelror, 2009).

The Carboniferous–Triassic Uralian orogeny in the east of the Barents shelf (Rickard & Belbin, 1980; Ziegler, 1988; Gee et al., 2006; Pease, 2011) and associated uplift provided a prominent sediment source for the Barents shelf. Large deltaic systems prograded from the southeast, and across the Barents Shelf and built out over earlier Triassic deep-marine deposits (Riis et al., 2008; Glørstad-Clark et al., 2010; Høy & Lundschien, 2011; Anell et al., 2014; Klausen et al., 2015).

The targeted reservoir section (Fig. 2) envisaged for the Longyearbyen CO_2 Lab belongs to the Upper Triassic to Middle Jurassic Kapp Toscana Group, which comprises the sandstone-dominated De Geerdalen Formation and the overlying Wilhelmøya Subgroup (i.e., the Knorringfjellet Formation; Worsley, 1973, 2008; Knarud, 1980; Mørk et al., 1982; Harland & Geddes, 1997; Mørk & Worsley, 2006; Mørk, 2013; Rismyhr et al., in press). The De Geerdalen Formation represents paralic deposition while the Wilhelmøya Subgroup was deposited in a deltaic, tide-dominated shoreline, and inner-shelf environments. Herein, the Wilhelmøya Subgroup is divided into three sequences after Rismyhr et al. (in press). Sequence 1 is broadly comparable to the Tverbekken Member and includes the Slottet Bed, sequence 2 is comparable to the Teistberget Member, while sequence 3 is comparable to the Brentskardhaugen Bed.

The reservoir units are overlain by a 450 m-thick, shale-dominated succession belonging to the Middle Jurassic to Lower Cretaceous Agardhfjellet Formation (Koevoets et al., 2016, 2018) and the Early Cretaceous Rurikfjellet Formation (Dypvik et al., 1991; Grundvåg et al., in prep.), which represents the regional caprock and seal for the targeted storage formation (Fig. 2). Overlying the reservoir-seal succession, the overburden continues with the 60 m-thick fluvial to deltaic deposits of the Barremian Helvetiafjellet Formation and 60 m-thick, Aptian to Albian, shallow-marine to inner-shelf deposits belonging to the Carolinefjellet Formation (Grundvåg et al., in prep.). The transition between the two formations is marked by an erosional unconformity related to crustal updoming driven by the HALIP event (Maher, 2001; Midtkandal et al., 2007; Nejbert et al., 2011; Minakov et al., 2012; Corfu et al., 2013; Senger et al., 2014a; Polteau et al., 2016). Mafic igneous intrusions (approx. 122.2–124.5 Ma) associated with the HALIP locally (Fig. 2) played an important role in terms of diagenesis and perhaps compartmentalisation of the Mesozoic sedimentary succession (Corfu et al., 2013; Senger et al., 2013, 2014a).

In the latest Cretaceous, a dextral transform fault zone known as the De Geer Zone (i.e., the palaeo-Hornsund Fault Zone) developed between Greenland and the western Barents Sea (Talwani & Eldholm, 1977; Gaina et al., 2009). Initial stages of break-up and sea-floor spreading were accompanied by a phase of Palaeogene transpression, which led to the development of the West Spitsbergen Fold-and-Thrust Belt (WSFTB; Braathen & Bergh, 1995; Bergh et al., 1997; Braathen et al., 1999; Leever et al., 2011). The WSFTB is characterised by a western thick-skinned province where structures are basement-involved, and a thin-skinned fold-thrust belt with three distinct detachment levels along weak

evaporite and shale intervals, two of which bound the Longyearbyen CO_2 reservoir (Fig. 2; Bergh et al., 1997; Braathen et al., 1999; Blinova et al., 2012). In addition, small-scale extensional structures (Fig. 2) seen to offset the storage formation (Lord, 2013; Ogata et al., 2014; Roy et al., 2014; Mulrooney & Braathen, 2015) have been related to differential tectonic loading during the evolution of the WSFTB crustal flexure. This flexure was induced by orogenic loading of the WSFTB which created the Palaeogene Central Tertiary Basin (CTB), a foreland basin accommodating sediments from the uplifted western hinterland and infilled by Palaeogene marine to continental facies (Steel & Worsley, 1984; Braathen et al., 1999; Helland-Hansen, 2010; Anell et al., 2014). The Longyearbyen CO_2 Lab study area (Fig. 2) is situated on the northwestern margin of the CTB. Vitrinite reflectance measurements by Throndsen (1982) suggest that the target formations in this study were buried to a depth of approx. 4.5 km, while a depth of approx. 3.7 km can be inferred from a more recent study by Marshall et al. (2015). This burial caused mechanical and chemical compaction that significantly altered the primary properties of the potential reservoir sandstones and cap-rock shales (Braathen et al., 2012; Senger et al., 2012; Mørk, 2013; Koevoets et al., 2018). The Longyearbyen CO_2 reservoir experienced approximately 3.5 km of uplift from the Oligocene, and mostly during the Late Miocene, Pliocene and Quaternary when Svalbard and the entire Barents Sea region were subject to significant glacial isostatic rebound and erosion (Dimakis et al., 1998; Bohloli et al., 2014). The development of severe underpressure within the study area is linked to the Cenozoic uplift and repeated glaciations (e.g., Wangen et al., 2016), though the extent of this and the main drivers are not fully understood.

Data and methods

The study presented herein utilised core and wireline log data from three closely spaced wells in Adventdalen (DH4, DH5R, DH7A) and an additional well 7 km to the northwest (DH2; Fig. 2), which fully penetrated the Wilhelmøya Subgroup. In addition, field studies were conducted 15 kilometres northwest of the Adventdalen well site (Drill site 2; Fig. 2) where the subgroup crops out. A summary of the multidisciplined approach to appraising the target reservoir is given in Table 1.

Core samples from boreholes and outcrops were collected for pore network characterisation (Fig. 3), and analysed using high-resolution X-ray computed tomography (micro-CT; Cnudde & Boone, 2013; Van Stappen et al., 2014). In order to fully characterise the pore network, micro-CT was then combined with other techniques, notably Mercury Intrusion Porosimetry (MIP; Cnudde et al., 2009) and Helium-porosimetry (HeP; Van Stappen et al., 2014). The analysis focused on the 3D pore structure and the presence of microcracks (Van Stappen et al., 2014). A more complete description of this methodology is described in Appendix 1.

High- and low-pressure water injection tests (Larsen, 2010, 2012; Senger et al., 2015a) were performed targeting the Wilhelmøya Subgroup (Fig. 4) to obtain permeability information and to test lateral communication between wells.

Effects of diagenesis and quartz cement distribution within the target reservoir were discerned by optical microscopy of 55 polished thin-sections, supplemented by scanning electron microscopy back-scattered electron image and energy dispersive analysis for mineral identification and microstructural interpretation (Mørk, 2013).

Structural analysis of the outcropping reservoir section was performed to improve the control of differential fracturing of litho-mechanical units as well as meso-scale (>50 cm displacement, subseismic) faults and igneous intrusions on fluid flow and reservoir compartmentalisation. Structural discontinuity mapping was conducted on the target succession outcrops where scan-lines (i.e., the line-intersection method; Singhal & Gupta, 2010) have been measured to provide horizontal fracture frequency plots along individual intervals, as well as fracture orientation, not available from the unorientated drillcores. Discontinuity classification is based on Schultz & Fossen (2008). In addition, meso-scale fault systems and associated damage zones were identified and mapped in terms of breccia series and gouge thickness/composition (Ogata et al., 2014; Mulrooney & Braathen, 2015). Fault architecture was mapped using virtual outcrop models created using photogrammetry, e.g., Buckley et al. (2016).

Clay gouge from 5 normal faults affecting the reservoir were sampled from outcrops in Konusdalen (Fig. 2) and subject to X-ray diffraction (XRD) mineralogical composition analyses. A background sample from a shale-rich bed within the Wilhelmøya Subgroup and outside of the fault damage zones was also analysed. The second part of the analysis attempted to model clay fraction aggregates. Analysis was run using a D8 advanced Bruker diffractometer equipped with Copper Ka radiation (40 kV and 40 mA) and LynxEye detector (expanded upon in Appendix 2).

Injection and fluid flow properties of the Wilhelmøya Subgroup were investigated by conducting water injection tests (Fig. 4) in DH7A (Test 1) and DH5R (Test 2). High- and low-pressure water injection tests (Larsen, 2010, 2012) were performed (Fig. 4) to obtain permeability information and to test lateral communication between wells. The first (Test 1) consisted of an active injection and falloff sequence in

Table 1. Summary of Longyearbyen CO_2 lab studies, methods and datasets.

Well appraisal				
Analyses	**Aims**	**Data sets**	**Resolution (m)**	**Key references**
Water injection and monitoring tests	Permeability information/ test lateral communication	Test results from 3 wells	~100 m	Larsen (2010, 2012)
Pore network characterisation				
Analyses	**Aims**	**Data sets**	**Resolution (m)**	**Key references**
X-ray computed tomography (Micro-CT)	Quantify fracture orientation, length and maximum aperture	12 Core plugs/ 12 outcrop plugs	≥2.8 µm	Cnudde & Boone (2013); Van Stappen et al. (2014)
Image reconstruction (Octopus software suite)	3D pore structure and (micro-) crack analysis	12 Core plugs/ 12 outcrop plugs	~1 µm	Van Stappen et al. (2014)
Mercury Intrusion Porosimetry (MIP)	Refinement of pore network characterisation	12 Core plugs/ 12 outcrop plugs	~1 µm	Cnudde et al. (2009)
Helium-porosimetry (HeP)	Refinement of pore network characterisation	12 Core plugs/ 12 outcrop plugs	~1 µm	Van Stappen et al. (2014)
optical microscopy	Effects of Diagenesis and quartz cement distribution	55 polished thin sections	~0.5 mm	Mørk (2013)
scanning electron microscopy / energy dispersive analysis	mineral identification and microstructural interpretation	Core samples	~1 µm	Mørk (2013)
Fault analysis				
Analyses	**Aims**	**Data sets**	**Resolution (m)**	**Key references**
Meso-scale fault systems	Determine fault attitudes, frequency, style	Outcrops, Virtual outcrop models	cm - 100 m	Ogata et al. (2014); Mulrooney & Braathen (2015)
Fault gouge analysis	Determine clay mineral composition and clay fractions	6 outcrop samples (locations in Fig. 6)	~1 µm	Mulrooney et al. (this volume)
Fracture Analysis				
Analyses	**Aims**	**Data sets**	**Resolution (m)**	**Key references**
Structural logging of cores	Determine physical characteristics and frequency distribution	4500 m of drill cores/ Optical televiewer	~1 cm	Ogata et al. (2012)
Line-intersection method, outcrops	Litho-mechanical control of fracture network	105 scan-lines, 7672 measurements	~1 cm	Ogata et al. (2014)
Igneous intrusion analysis				
Analyses	**Aims**	**Data sets**	**Resolution (m)**	**Key references**
Regional igneous study	Determine geometries of igneous intrusions	Seismic, magnetic, LIDAR and borehole data	≥10 m	Senger et al. (2013)
Igneous affects on reservoir	Impact of igneous intrusions on reservoir properties			
Sedimentological analysis				
Analyses	**Aims**	**Data sets**	**Resolution (m)**	**Key references**
Sedimentological study	Facies analysis, seq. strat, palynology of the reservoir	4 drill cores/ outcrop logs	~1 cm	Rismyhr et al. (this volume)

DH7A over a 9-day period starting Sept. 6, 2012, followed by an extended falloff for 310 days ending July 21, 2013, with possible pressure interference monitored in DH5R, 94 m away. The test sequence was run for 4 hours with injection rates of up to 368 m^3/d followed by 22.6 hours of shut-in, for 0.36 hours with injection rates of up to 1363 m^3/d followed by 42 hours of shut-in, for 5.8 hours with injection rates of up to 1373 m^3/d followed by 71.4 hours of shut-in, and finally 72.2 hours with injection rates of up to 476 m^3/d (451 m^3/d the last 13.5 hours) followed by an extended falloff interval that lasted 7432 hours (approx. 10 months). The second injection and falloff test (Test 2) was conducted in DH5R (Larsen, 2012; UNIS CO_2 lab AS, 2015) with 2 days of injection

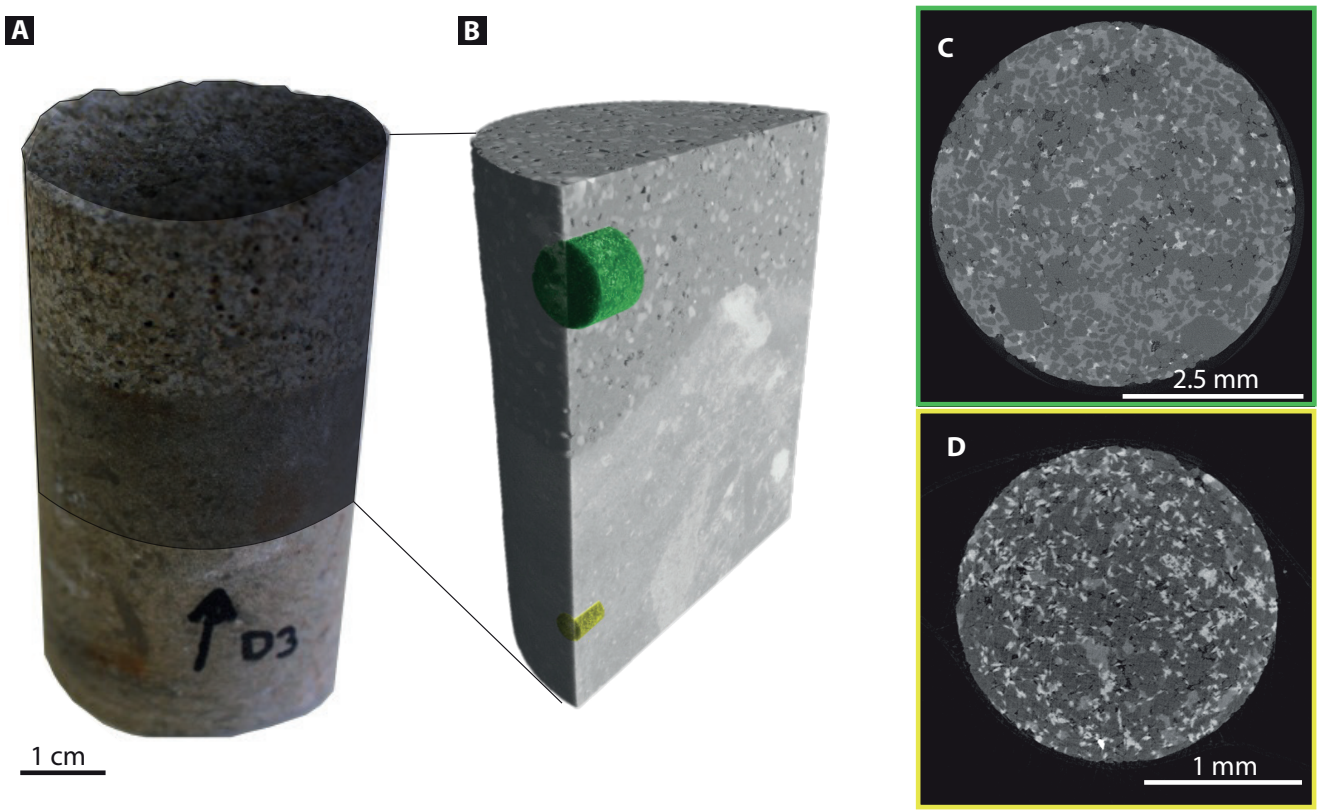

Figure 3. *Principle of down sampling for the CT-scanning technique, illustrated with a drillcore sample (A) from DH2, taken at depth of 752.34 m. The drillcore sample (diameter 42 mm) was initially scanned at a resolution of 60 µm, in which a sudden change in lithology is present (B). Based on this rendering, smaller subsamples (5 mm and 3–4 mm diameter) were taken, which could be analysed at resolutions of 4 µm and 2.8 µm, respectively, illustrated by the 2D slices in (C) and (D), respectively.*

starting on Aug. 11, 2014 and followed by an 848 hour-long falloff period ending Sept. 17, 2014. The injection rate was kept stable at approx. 310 m^3/d for 40 hours, after which the rate was gradually increased to 325 m^3/d over an 8-hour period.

Results

Flow and shut-in tests

Test 1

Injection and falloff results from DH7A are shown in Fig. 5, with a log-log diagnostic plot in Fig. 5A of test data from the extended falloff (markers) and data from an analytical model (curves) with a uniform-flux fracture (i.e., uniform inflow over the entire fracture area) with half-length xf = 83 m orientated parallel to a flow barrier 58 m from the well, and a test overview plot in Fig. 5B of the entire data set from DH7A (markers) along with output from the analytical model (curve). The green markers in Fig. 5A represent pressure changes after shut-in, while the red markers represent semi-log derivatives after shut-in. The derivatives are used to identify the flow response, with the 45 degree climb between 0.4 and 100 hours into the falloff typical for flow along a fracture enhanced by boundary effects from the nearby flow barrier, and the flat part indicated at the end typical for radial flow (in this case from a half-circle due to the flow barrier on one side). Apart from the first half hour, the match of test data and model output is excellent. Given a reservoir thickness of approx. 24 m (determined from outcrops; Ogata et al., 2014), a permeability of 2.55 md is obtained from a flow capacity of 61.2 md·m referred to above.

The results (Fig. 5) of the first test show very limited to no pressure communication between DH5R and DH7A, which implies that there must be flow barriers in the subsurface. In addition, test results for DH7A are consistent with injection-related hydraulic fracturing (i.e., DH7A is a fractured well) and the presence of a nearby flow barrier. Since it is often difficult to identify radial flow data from fractured wells, it can be challenging to obtain good estimates of the flow capacity (i.e., the kh product). However, with almost 8000 hours of shut-in data from DH7A, a flow capacity of 61.2 md·m can be determined with a high degree of confidence. Results are less certain for determining the fracture half-length (xf in Fig. 5) and the distance to the flow barrier, but values outside the range 70–100 m for the half-length and 50–60 m for the distance are not likely. These

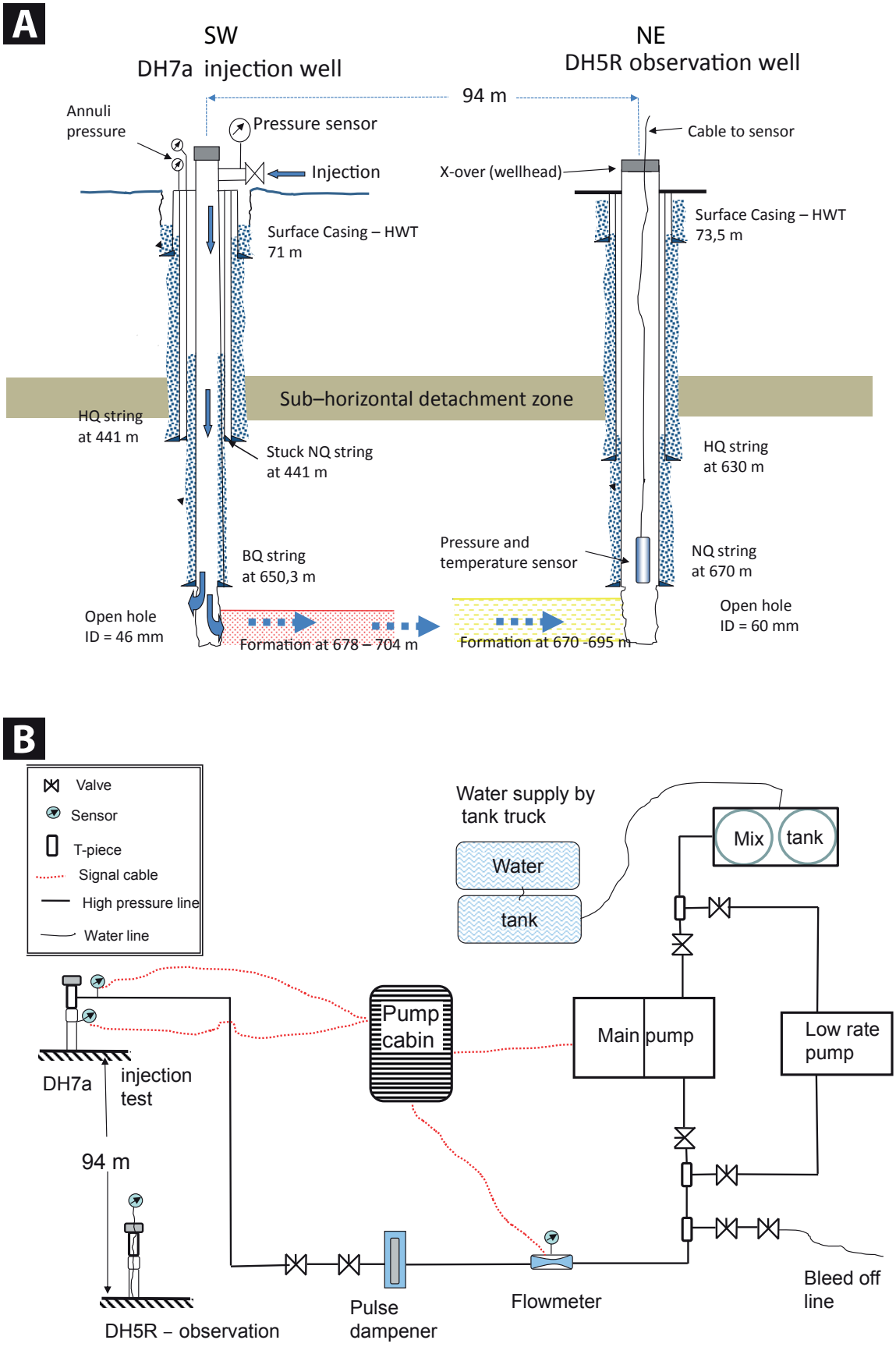

Figure 4. Well design and flow chart for the fluid flow tests. (A) Schematic depiction of the water flow test conducted on the Wilhelmøya Subgroup with well DH7A as the injector and DH5R as the observation well. The down-hole pressure gauge in DH5R was placed at 645 m. Abbreviations: HWT – Well into bedrock, HQ – 66 mm casing, NQ – 56 mm casing, BQ – 46 mm casing, ID – Internal diameter. Blue stippling is cement. (B) Technical diagram for the water test provided by Baker Hughes.

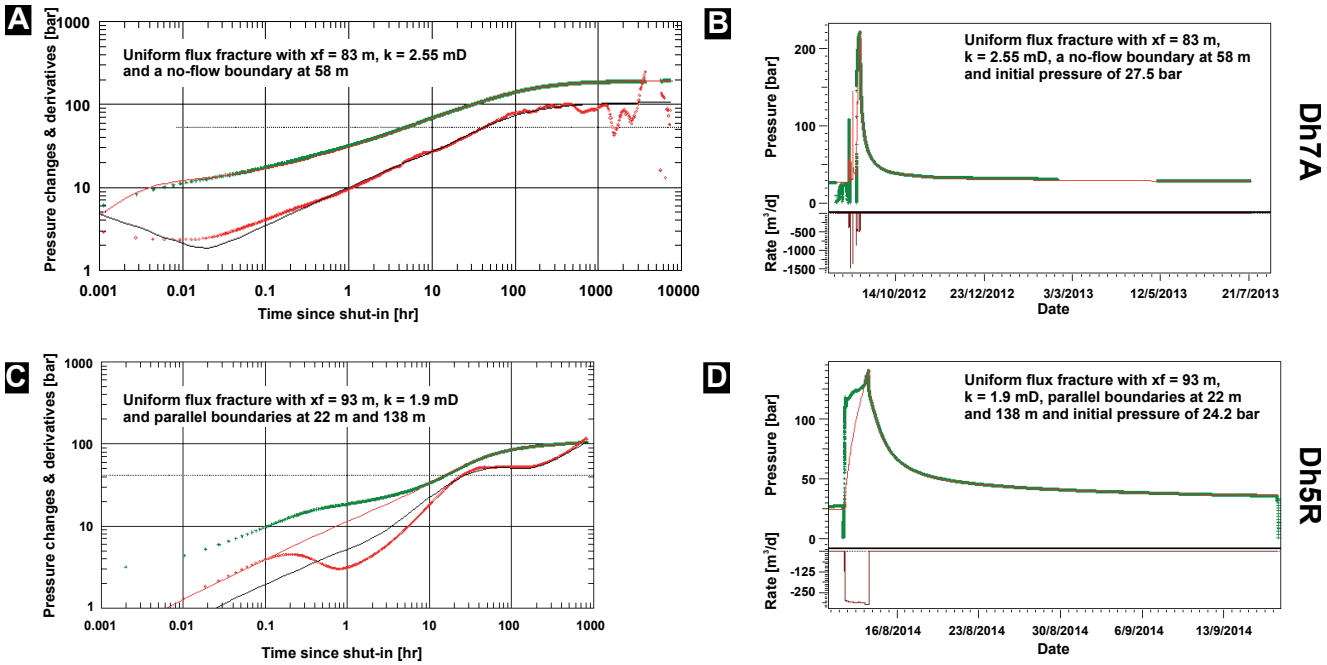

Figure 5. Flow and shut-in test results from the Wilhelmøya Subgroup in Adventdalen. (A) Log–log match of the extended DH7A falloff (test 1) with a uniform-flux fracture and a sealing boundary. Observed pressure change after shut-in (green markers). Modelled pressure change after shut-in (red curves). Semi-log derivates (red markers). Modelled semi-log derivitives (black curves). Abbreviation: xf – fracture half-length, K - permeability. (B) Match of the entire DH7A dataset with the uniform-flux fracture and sealing boundary. Y-axis showing both pressure (bar) and flow rate (m^3/d). (C) Log–log match of the DH5R falloff data (test 2) with a fractured off-centre well in a linear flow unit. Observed pressure change after shut-in (green markers). Modelled pressure change after shut-in (red curves). Semi-log derivates (red markers). Modelled semi-log derivatives (black curves). (D) Match of the entire DH5R dataset with the fractured off-centre well in a linear flow unit. Y-axis showing both pressure (bar) and flow rate (m^3/d).

uncertainties are related to unknown flow properties within the induced fracture.

In the analysis, the flow barrier has been modelled as fully sealing, but the DH7A data are also consistent with some minor leakage across the boundary, e.g., with a multiplier lower than 0.01. A multiplier in this range is also consistent with the lack of observable interference in DH5R, especially with unstable and noisy data in DH5R after well operations with falling water level coupled with variable gas influx in DH5R (Huq et al., 2017). Poor reference data, as in this case, require a strong response to be clearly identifiable as interference, as with no barriers or barriers with only moderate flow restrictions. Pressure data were monitored for almost two years in DH5R, until May 5, 2014, but beyond the first few weeks the response was clearly dominated by gas influx.

A key observation from the DH7A data is that the Wilhelmøya Subgroup is under-pressured by at least 35 bar with reference to standard sea level.

Test 2

In contrast to the DH7A data from the first test, the extended falloff from DH5R is difficult to match with a single model. The log-log diagnostic plot in Fig. 5C shows a chosen match of falloff data from DH5R with a fractured well between parallel no-flow boundaries. Although the model does not match early data, a good match is obtained for the last 830 hours of the falloff. The results listed in the plot, with a uniform-flux fracture with a half-length of 93 m, permeability of 1.9 md, and the presence of no-flow boundaries (e.g., impermeable fractures) at 22 and 138 m from the well, are based on an assumed reservoir thickness of 30 m. These results are consistent with the DH7A results (Fig. 5A). The uniform-flux fracture has also been oriented parallel to the boundaries in the model. The reason for this 'channel-like' model used for DH5R is the upturn seen in derivatives (the lower data) after about 200 hours. The poor match of the early data shown in Fig. 5C is likely caused by a lack of fracture stabilisation during the single injection period prior to the falloff. This is evident in the history plot shown in Fig. 5D, where the uniform-flux fracture length is only consistent with the pressure response at the end of the injection period. In order to match the first part of the injection data, a shorter uniform-flux fracture would be needed. The same can be observed in the DH7A data over a shorter time scale, but not evident in Fig. 5B with almost 1 year of data. Although fracture propagation is evident in both datasets, a key difference is that a much larger volume was injected in DH7A (test 1) compared with DH5R (test 2) prior to the long shut-ins.

It is important to note that the initial pressure of 24.2 bar at a depth of 645 m listed in Fig. 5D corresponds to the value needed in the analytical model to match the test data from DH5R. Since the model does not fully match the data, there is some added uncertainty about the formation pressure in DH5R. Since the recorded pressure was 27.5 bar and rising prior to the start of injection, it is most likely that the initial pressures were the same at the two well locations, e.g., 29.9 bar at 670 m depth, and hence similarly under-pressured.

Faults in the target successions

The presence of subsurface, potentially baffling faults within the target reservoir is consistent with outcrop and seismic observations throughout central Spitsbergen. Normal faults are observed along the coast of western Spitsbergen, e.g., the Forlandsundet Graben (Steel et al., 1985; Gabrielsen, 1992), as well as offshore (Eiken & Austegard, 1987). Similar structures are described on the eastern flank of Boret Mountain, central Spitsbergen and within the Svea mine (locations shown in Fig. 1; Goss, 2013). In the latter case, thrusts related to the WSFTB (Bergh et al., 1997; Braathen et al., 1999) form the sole to the extensional faults where both structures are envisaged to have formed contemporaneously.

Meso-scale faults, defined herein as faults that have >50 cm displacement, are subseismic (Ogata et al., 2012, 2014; Roy et al., 2014; Mulrooney & Braathen, 2015) and affect the reservoir successions in a N–S-trending river section 15 kilometres northeast of the drill sites. The Konusdalen fault system, illustrated in Fig. 6, affects the uppermost part of the De Geerdalen Formation (Isfjorden Member) and the entire Wilhelmøya Subgroup. Here, these faults exhibit strikes of NE–SW to ENE–WSW, and dip approximately 65° towards the NW to NNW. Antithetic faults are also present, and dip approximately 70° towards the SE to SSE. The Konusdalen outcrop consists of 3 rotated fault blocks ranging from 2 to 6 metres in width, and is characterised by a 2 m-wide graben and an 11 m-wide horst. Five faults and associated splays are identified: the K1, K3 and K5 faults consist of several synthetic and antithetic segments, some discontinuous. The majority of fault displacement is accommodated by narrow zones of penetrative strain, i.e., fault cores. In one case, K3, an example of down-section bifurcation is observed (Fig. 6B). Fault zones K2 and K5, in contrast, are defined by single discrete slip surfaces. Maximum displacement on individual faults is approximately 3 m.

Each fault core is surrounded by a damage zone, i.e., a volume of deformed wall rocks around a fault core or slip surface that results from the initiation, propagation, interaction and build-up of slip along faults (e.g., Cowie & Scholz, 1992; McGrath & Davison, 1995). The fault core and damage zones in Konusdalen can be described in terms of breccia series, fracture frequency and gouge presence following Braathen et al. (2004, 2009). Country-rock brecciation (protobreccia, breccias or ultrabreccia) and gouge are displayed in Fig. 6D. Away from zones of brecciation and fault induced fracturing, background fracturing (Fig. 6C) is observed. Deformation varies between fault zones; for example, K1 is characterised by a discrete gouge-cored fault zone surrounded by relatively undeformed country rock. In contrast, faults K3a and K4 show undulating zones of coarse-grained gouge and breccias spanning a 25 cm envelope around the fault's core. Fault zones K3 and K5 are characterised by thick, but undulating (max. 75 and 22 cm, respectively) zones of variably brecciated rock. In addition, lenses comprising lesser localised brecciation are in places rafted within more mature brecciated fault rock, and envisaged to have been broken off from the fault-core walls during slip events. The damage zones shown in Fig. 6 range between 1 and 4.5 m width for individual faults. The presence of undulating clay gouge in fault cores is likely derived from the low N/G ratio (25–50%) host-rock succession. The gouge forms clay abrasion membranes of variable thicknesses, but no true development of shale-smear is present.

Results of X-Ray diffraction (XRD) analyses of gouge sampled from five fault cores (K1, K2, K3, K4 and K5) are summarised in Table 2. The gouge is not completely formed of clay minerals, containing between 23 and 43% quartz. The cores are typically characterised by gouge containing (in descending abundance) quartz, muscovite/illite, plagioclase, kaolinite and chlorite. Some fault cores also contain small volumes of microcline, siderite, pyrite and apatite. The composition of the gouge is broadly similar to that of shale- and claystone-rich beds of the Wilhelmøya Subgroup (sequence 1). Clay fraction modelling, in addition to chlorite-smectite (C–S) and mixed layer Illite-smectite (I–S) ratios are shown in Table 3. The increased I/S ratio in the fault gouges in comparison to the host rock, apart from K3, may be indicative of shear-stress-induced dehydration, which makes smectite highly reactive and prone to transform into illite (Casciello et al., 2004). The progressive transformation of smectite to illite via mixed-layer illite/smectite (I/S) correlates with changes in temperature due to burial depth, although the function curve for this process is very coarse (Kubler, 1967; Hower et al., 1976; Boles & Franks, 1979; Pollastro, 1993; Árkai et al., 2002). Other factors, such as geotectonic setting, period of heating, rock composition, porosity, fluid circulation, and K^+ ion availability, can also influence these parameters (Frey, 1987; Merriman, 2005; Dellisanti & Valdrè, 2008; Merriman & Peacor, 2009; Dellisanti et al., 2010). Assuming a hyperthermal gradient of 50°C/km (Marshall et al., 2015) owing to the presence of dolerite intrusions (Senger et al., 2014a), and burial to approx. 3.7 km (see above), the target reservoir experienced temperatures of approximately 185°C (Marshall et al., 2015). This high temperature is supported by observations of pervasive quartz cementation (Mørk, 2013).

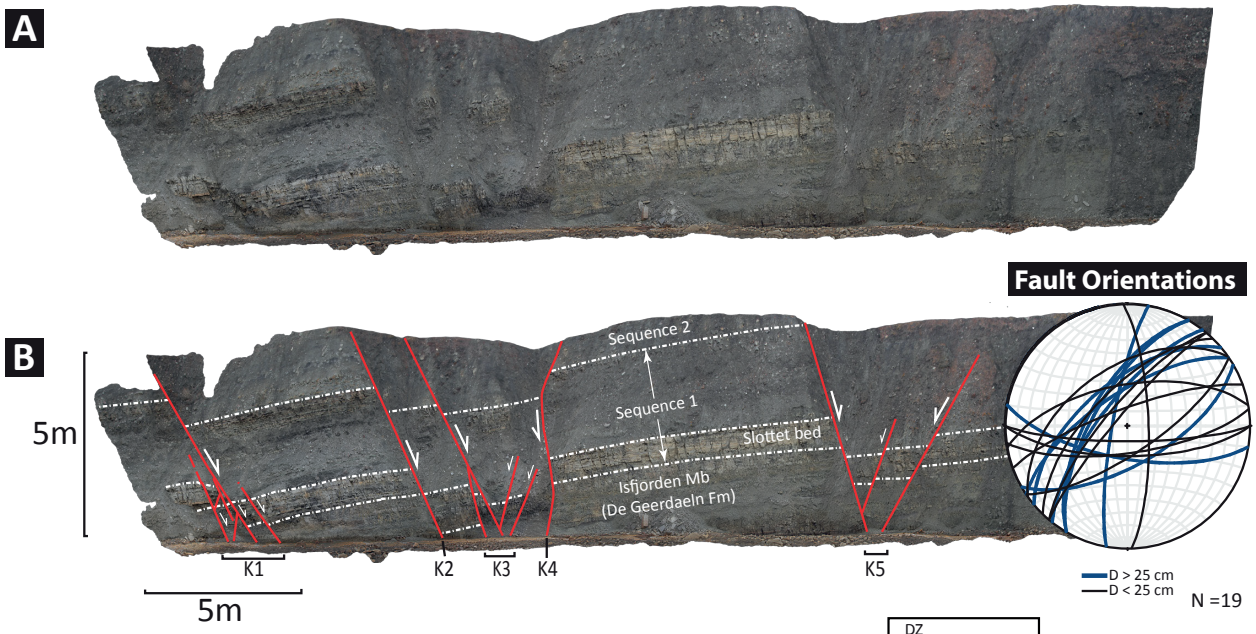
A
B
5m
Sequence 2
Sequence 1
Slottet bed
Isfjorden Mb
(De Geerdaeln Fm)
K1
K2
K3
K4
K5
5m
Fault Orientations
D > 25 cm
D < 25 cm
N =19

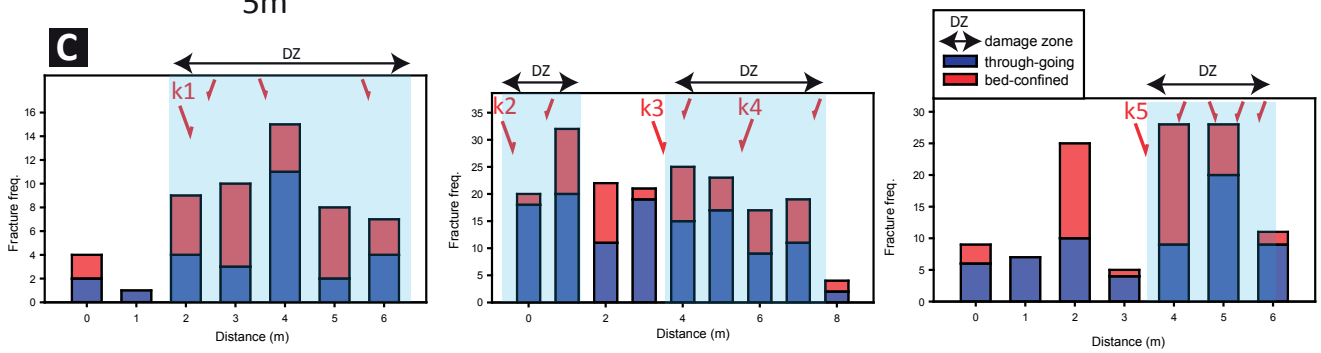
C
DZ
damage zone
through-going
bed-confined
k1
k2
k3
k4
k5
Fracture freq.
Distance (m)

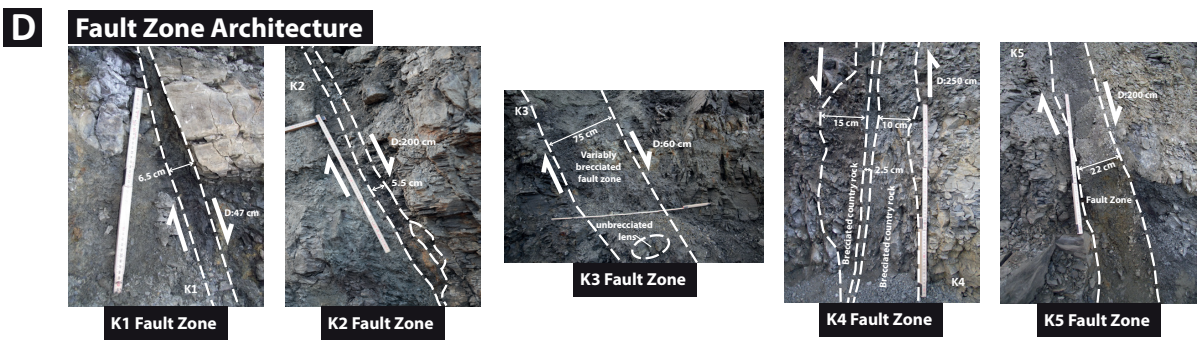
D
Fault Zone Architecture
K1 Fault Zone
K2 Fault Zone
K3 Fault Zone
K4 Fault Zone
K5 Fault Zone

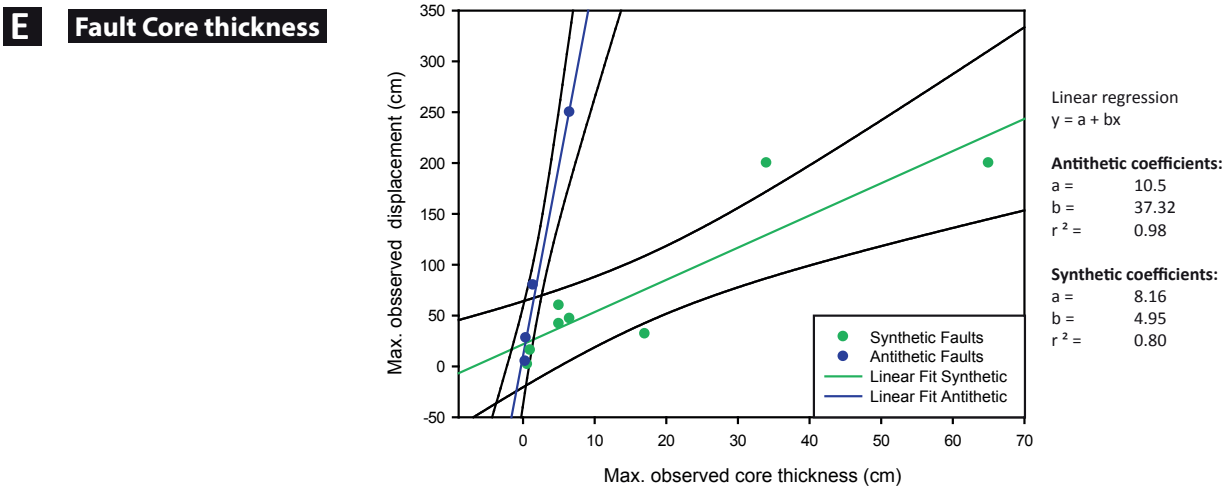
E
Fault Core thickness
Max. obsserved displacement (cm)
Max. observed core thickness (cm)
Synthetic Faults
Antithetic Faults
Linear Fit Synthetic
Linear Fit Antithetic
Linear regression
y = a + bx
Antithetic coefficients:
a = 10.5
b = 37.32
r ² = 0.98
Synthetic coefficients:
a = 8.16
b = 4.95
r ² = 0.80

Figure 6. (A) Photogrammetric mosaic of the extensional fault system affecting the Wilhelmøya Subgroup that crops out in Konusdalen (location shown in Fig. 2). (B) Interpretation of faults, slip directions and main litho-stratigraphic features. The inset stereoplot shows that the normal faults predominately strike NE–SW to ENE–WSW and have displacements down to the NW to NNW. Antithetic faults are also present. (C) Fault damage zones are characterised by increased fracture frequency and range between 1 and 4.5 metres in width. (D) Images of architectures of the fault zones showing fault zone brecciation. Fault cores are characterised by undulating clay gouge of variable thickness, the maximum observed thickness of which is plotted against the observed displacement on slip surfaces (E). Dashed lines in (D) highlight boundaries between fault facies, arrows show fault kinematics, D – fault displacement in cm, double-headed arrow – fault facies element width.

Faults affecting the lower part of the Agardhfjellet Formation are observed in a valley section 3 km to the east of Konusdalen (Fig. 7; Ogata et al., 2014; Mulrooney & Braathen, 2015) in Criocerasdalen, and in an unnamed valley 1 km west of Criocerasdalen (location in Fig. 2). These faults are, however, not hard linked to the aforementioned Konusdalen system, i.e., they tip out towards the base of the Agardhfjellet Formation. Correspondingly, the Konusdalen faults tip out up-section approx. 10 m below the interface between the Wilhelmøya Subgroup and the Agardhfjellet Formation. In addition, faults affecting both successions show some notable geometrical contrasts, i.e., spacing and dip (Fig. 8). Konusdalen faults are closely spaced (1–10 m spacing) and show steep dips in the range of 65–85°, whereas Criocerasdalen faults display spacing in the range of 25 and 45 m, low-angle 25° dipping synthetic faults and steeper, 60° dipping, antithetic faults. Moreover, the Criocerasdalen faults strike approximately 10° counter-clockwise of the underlying systems.

The varying styles of faulting affecting the caprock and reservoir sections along with similar discrepancies in fracture trends observed by Ogata et al. (2014) are likely caused by vertical geomechanical variation in the stratigraphic succession, not least controlled by a notable transition from the heterolithic Wilhelmøya Subgroup into the shale- and claystone-dominated Agardhfjellet Formation. The transition also stratigraphically correlates to a variation in fracture pressures identified in well tests (Bohloli et al., 2014).

Natural fracture systems

Open natural fractures (unrelated to injection or drilling operations) within the Wilhelmøya Subgroup have been shown to contribute to permeability, fluid injectivity and storage capacity. Fractures are identified in both outcrop and in drillcores (Fig. 9; e.g., Ogata et al., 2012, 2014), and their genesis is primarily attributed to Palaeogene transpression during evolution of the WSFTB and subsequent uplift and unroofing. Locally, enhanced fracturing occurs in damage zones of the Konusdalen fault system as described above and in the vicinity of igneous intrusions (Senger et al., 2014a, b). Due to the low matrix permeability, it is critical to

Table 2. X-ray diffraction (XRD) Reitveld refinement results showing bulk composition of gouge samples from five fault cores (K1 to K5) and from a single sample (W1) from a shale-rich bed of the Wilhelmøya Subgroup (sequence 1).

	Quartz (%)	Muscovite/Illite (%)	Chlorite (%)	Kaolinite (%)	Microcline (%)	Plagioclase (%)	Siderite (%)	Pyrite (%)	Apatite (%)
K1	38,5	25,43	1,42	15,9	n/a	18,69	n/a	n/a	n/a
K2	43,01	21	7,64	1,98	n/a	18,45	7,93	n/a	n/a
K3	23,13	19,39	2,16	***5,27***	n/a	8,49	33,76	1,606	3,69
K4	**40,56**	**28,45**	**2,49**	**9,09**	**1,19**	**16,89**	**1,32**	**n/a**	**n/a**
K5	38,66	32,21	n/a	10,64	3,72	14,77	n/a	n/a	n/a
W1	39,3	31,31	2,99	15,02	2,61	8,19	n/a	0,576	n/a

Table 3. Results of NEWMODE II clay fraction modelling.

Sample	[1]Illite	[2]Chlorite	[3]Kaolinite	[4]Chlorite-Smectite (R1)	[5]mixed layer Illite-smectite (R0)
K1	49,1	1,0	24,8	0,7	24,3
K2	48,7	2,3	25,4	1,0	22,6
K3	43,0	1,1	36,0	***2,2***	17,8
K4	**63,7**	**6,5**	**5,3**	**0,4**	**24,0**
K5	66,1	0,0	7,7	0,9	25,3
W1	41,3	0,7	37,1	1,8	19,1

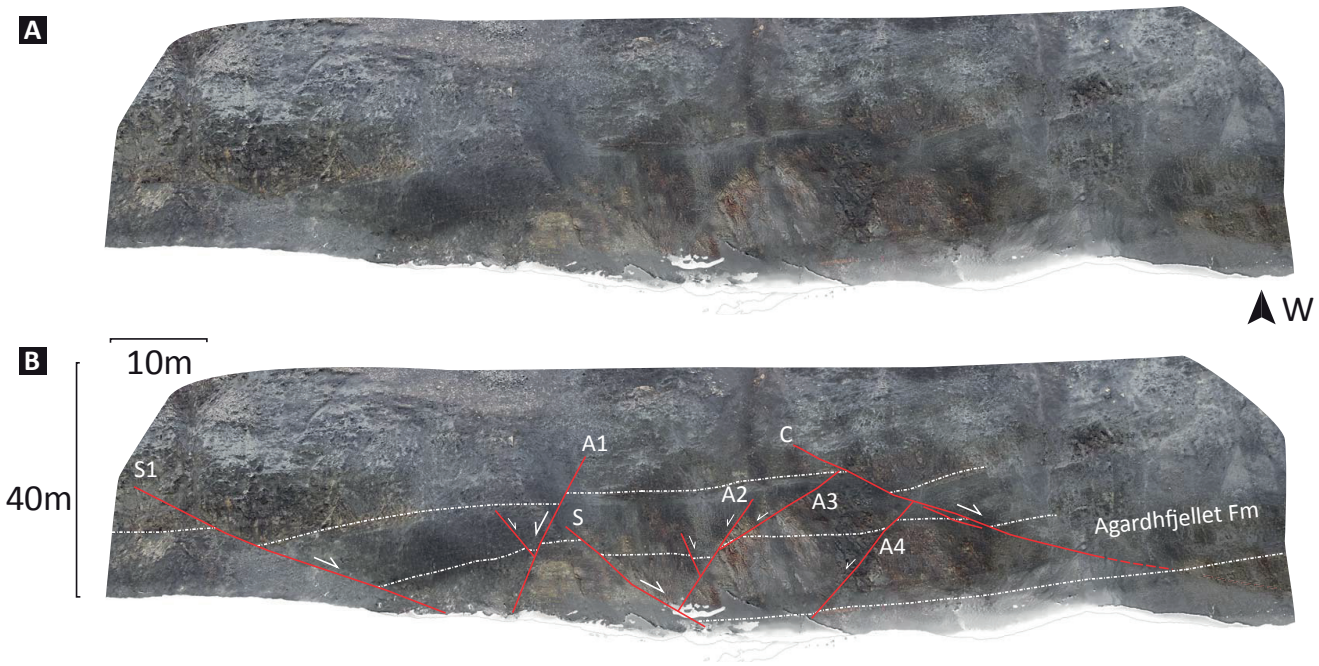

Figure 7. (A) Photogrammetric mosaic of the extensional fault system affecting the Agardhfjellet Formation that crops out in Criocerasdalen (location shown in Fig. 2). (B) Interpretation of faults and slip directions. S – synthetic, A – antithetic. Similar to the faults affecting the Wilhelmøya Subgroup, the Criocerasdalen faults predominately strike NE–SW to ENE–WSW and have displacements down to the NW to NNW. Synthetic faults are shallower than their Konusdalen counterparts (65–85° vs. 25°), while antithetic faults show comparable dips (approx. 60°). Spacing between faults is also wider in Criocerasdalen (more than double; see Fig. 8).

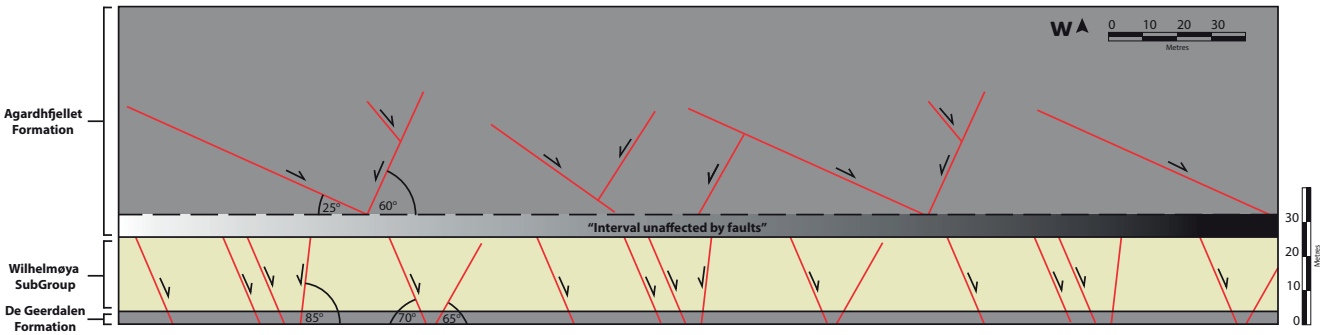

Figure 8. Schematic representation of the extensional fault system of Figs. 6 & 7 showing variations between a steep-dipping, narrow-spaced fault system within the Wilhelmøya Subgroup and a shallower dipping, widely spaced system within the Agardhfjellet Formation.

understand the nature of the fracture network from both field and injection data to accurately predict the likely CO_2 distribution in the subsurface. In this section, we outline the fracture heterogeneities at various scales (from micro-CT to meso-scale faults) and discuss their significance with respect to dynamic pressure data obtained from the boreholes.

Natural fractures in drillcores and outcrops

The significance of natural fractures in contributing to injectivity and fluid flow has been quantified during an open-hole water injection test in the underlying De Geerdalen Formation at 870–970 m in DH4 (Braathen et al., 2012; Ogata et al., 2012; Senger et al., 2015a). Following this test, the calculated permeability exceeded the measured matrix permeability by approximately one order of magnitude, with the enhanced injectivity attributed to an extensive natural fracture network. In the upper part of the reservoir, in the Wilhelmøya Subgroup, the matrix porosity and permeability is significantly higher than in the De Geerdalen Formation (Magnabosco et al., 2014), but the fracture network is nonetheless envisioned to enhance injectivity and provide fluid flow access to the secondary porosity. Furthermore, the fracture network may contribute up to 2.5% of the total storage resource estimate (Senger et al., 2015a).

The natural fracture network has been quantitatively characterised in terms of its density, orientation and relationship to the sedimentary succession (Ogata et al.,

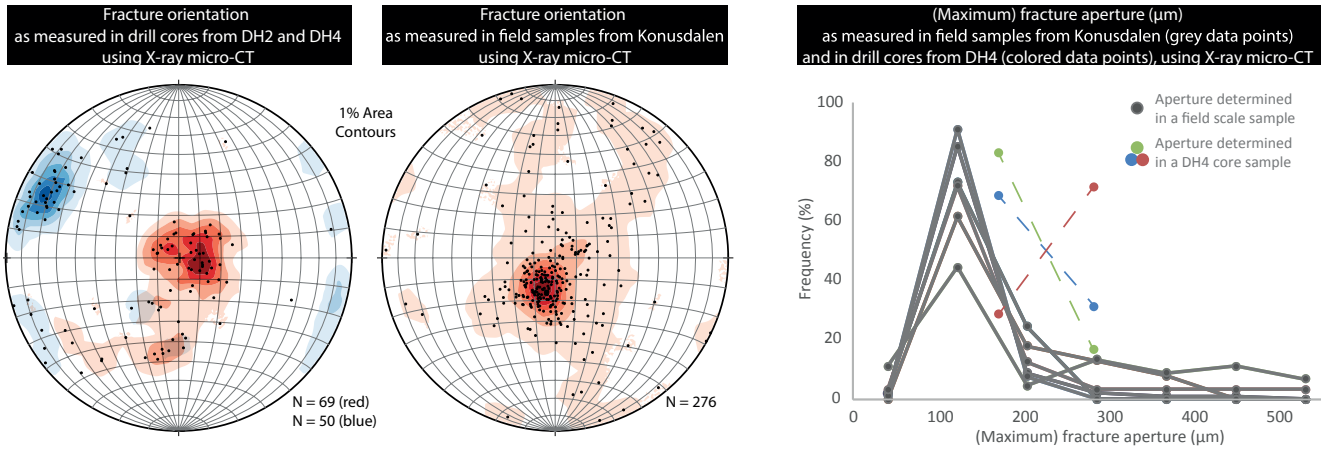

Figure 9. *Fracture orientation and maximum aperture as determined in both drillcore samples (stereoplot to the left, and coloured data points in the fracture aperture plot), as field samples from Konusdalen (stereoplot to the right and grey data points in the aperture plot). The stereoplots show the poles to the fractures. It is important to note that these plots should only be interpreted according to the dip of the fractures, since the scanned cores were not oriented. The maximum aperture distribution measured in the CT scans is shown to the right.*

2014). Drillcores, wireline logs and outcrop data were integrated to produce a conceptual model involving five litho-structural units (LSU) characterised by intrinsic fracture associations and lithological properties (Fig. 10; Ogata et al., 2014). Over 7500 individual fracture measurements were acquired in the field, primarily to determine the dominant fracture orientations. Two main fracture sets have been identified, namely an ENE–WSW-trending principal fracture set (parallel to faults discussed above) and a NNW–SSE-trending subordinate fracture set (Fig. 10B). This implies a potential for generating an asymmetric CO_2 plume governed both by the matrix permeability, the fracture permeability and the overall regional tilt of the reservoir. Finally, the fracture orientation analysis (Ogata et al., 2012, 2014) suggests that reservoir sandstones (i.e., LSU C; Fig. 10) will act as preferential vertical fluid migration pathways, while shale-dominated successions (i.e., LSU A; Fig. 10) will preferentially form lateral fluid migration pathways and enhance intraformational baffling

Micro-CT analysis

Micro-CT analysis offers a way to visualise the pore structure and pore size distribution inside rocks (e.g., Cnudde & Boone, 2013; Van Stappen et al., 2014, 2018). However, since it is limited in resolution, it has to be combined with other techniques such as Mercury Intrusion Porosimetry (MIP). This approach is illustrated in Fig. 11, in which a conglomerate sample of the Toarcian–Bajocian Brentskardhaugen Bed in DH4 (at a depth of 677.15 m) was analysed. The initial He-porosimetry measurements showed a porosity of 15.3%. The sample was scanned at a resolution of 56.6 µm, which allowed a subsample to be chosen in the area of the drillcore with the highest expected porosity. This subsample core was drilled with a diameter of 6 mm, allowing a scanning resolution of 4 µm.

For fracture characterisation, additional image analysis tools were applied complementary to previous studies (Van Stappen et al., 2014). This allowed the fractures within the retrieved samples to be analysed for their maximum aperture, length and relative orientation. Previous observations relating fracture occurrence to competence contrasts in sandstone and clay layers (Ogata et al., 2012, 2014) could be confirmed at the pore scale level (Van Stappen et al., 2014).

A comparison between fractures present in field samples and in the drillcores reveals some variations in fracture characteristics. Micro-CT analysis shows a clear difference in fracture length between the outcrop fractures and those analysed in the drillcores (Van Stappen et al., 2014). Generally, the fractures in the field samples are found throughout the entire diameter of the cylindrical samples and must thus be considered as a minimum length, whereas the length of fractures is limited in core samples to a maximum of 2.1 cm. Fracture apertures, on the other hand, were found to be similar in outcrop and core samples, with most apertures ranging between 123 and 283 µm (Fig. 11). Fracture orientations are predominantly horizontal to subhorizontal (Fig. 11), although these fractures are sometimes connected by a population of vertical fractures (Van Stappen et al., 2014). There is a small discrepancy between the absolute values of the measured fracture apertures for field and drillcore samples (Fig. 11).

Igneous bodies

Early Cretaceous igneous intrusions, U–Pb dated to c. 124.5 Ma, are present throughout Svalbard and especially in central Spitsbergen (e.g., Nejbert et al., 2011; Corfu et al., 2013; Senger et al., 2013, 2014b, 2015b). The mafic

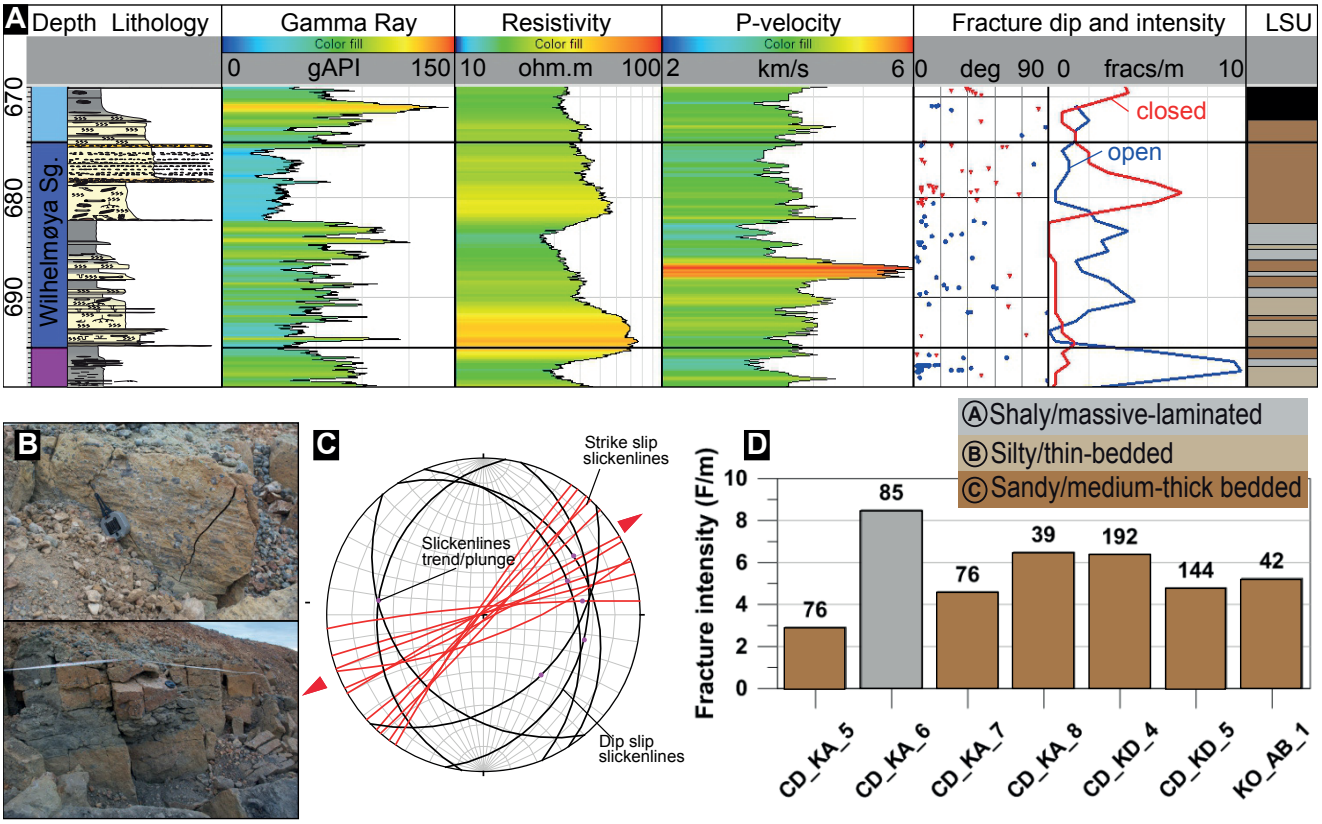

Figure 10. *Synthesis of structural information in the Wilhelmøya Subgroup from DH4 and relevant outcrops. (A) Wireline and core-based characterisation of the Wilhelmøya Subgroup in the DH4 borehole. The fracture dip and intensity plots are based on manual fracture counting reported by Ogata et al. (2012). (B) Typical outcrop appearance of the Wilhelmøya Subgroup lithologies, illustrating pervasive fracturing. (C) Orientation of slickenlines on two scanlines within the Wilhelmøya Subgroup (CD_KD_4 and CD_KD_5), illustrating a predominant WSW–ENE trend attributed to Paleocene transpression. This trend is also the dominant orientation of joints and fractures within the entire Kapp Toscana Group reservoir (from Ogata et al., 2014). (D) Average fracture intensity in 7 scanlines within the Wilhelmøya Subgroup from Ogata et al. (2014). On average, horizontal fracture intensity varies from 4 to 6 fractures/metre, but is anomalously higher in the shale-dominated CD_KA_6 scanline. The numbers indicate the amount of individual fractures measured at each scanline.*

intrusions, collectively referred to as the Diabasodden Suite (Dallmann, 1999), are all genetically linked and form part of the High Arctic Large Igneous Province (HALIP; Maher, 2001). The igneous bodies primarily form sills, typically less than 50 m thick but extending over 10 km laterally (Senger et al., 2014a). Subordinate dykes, transgressive sill segments and saucer-shaped intrusions are also present (Senger et al., 2013). Stratigraphically, the thickest sills are emplaced below the target reservoir as evident from borehole, outcrop and seismic observations (Bælum et al., 2012; Senger et al., 2013). Senger et al. (2014a) reported a 2.28 m-thick sill near the base of the DH4 borehole at 949.71–941.99 m depth with an associated contact metamorphic aureole, while Bælum et al. (2012) interpreted a high-amplitude reflection beneath the base of the DH4 borehole at 972 m as a much thicker sill, analogous to thick sills outcropping in the equivalent exposed stratigraphic interval at Hatten, approximately 18 km northeast of the DH4 borehole (i.e., within the lower De Geerdalen Formation). In addition, the presence of a solitary, thin (approx. 5 m thick) dolerite dyke at Botneheia (see Fig. 2 for location) extending through the entire Kapp Toscana Group into the overlying Agardhfjellet Formation caprock shales, shows that the entire thickness of the target successions is likely to be locally affected by small-scale intrusions. The directionality of the intrusions, especially where they occur as dykes, shows affinity towards two main trends, northwest–southeast and northeast–southwest. Contact aureoles documented by Senger et al. (2014a), and credited to heat conduction, show that a distance of up to 195% of the sill thickness has been geochemicaly and mechanicaly perturbed. To the east, on the island of Wilhelmøya, Haile et al. (2018) have credited hydrothermal circulation for the hydrothermal alteration of the reservoir succession a distance of over 500% of the thickess of sills. In places, this diagenesis shows reservoir temperatures locally reached approx. 140°C compared with more regional temperatures of 60–70°C driven my burial.

Reservoir characteristics and properties

Net gross; sandstone-shale ratio

A summary diagram showing a synthesis of reservoir

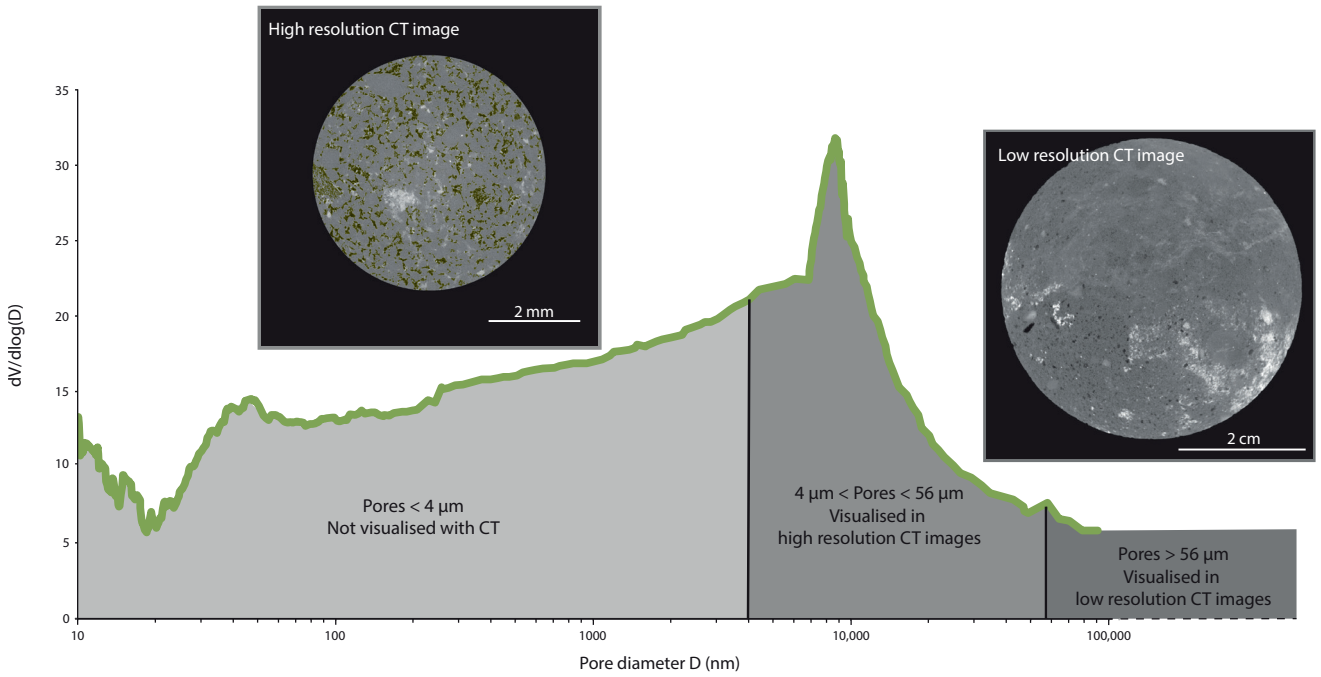

Figure 11. *Pore scale/space analysis of the Brentskardhaugen Bed conglomerate core sample from DH4 (depth = 677.15 m), through a combination of micro-CT analysis and MIP measurements (after Van Stappen et al., 2014). The specific intrusion volume dV (mm³/g) is given as a function of the pore diameter D (µm). Two micro-CT slices are given: a low-resolution CT scan, to the right (obtaining a resolution of 56 µm), in which a distinction could be made in high-porous zones and low-porous zones; and a high-resolution one after a subsample was taken, to the left, which was scanned at the resolution of 4 µm, in which the pores are more distinguishable. In the latter, which corresponds to the pore diameter interval of 4–56 µm in the MIP data, pores greater than 4 µm could be differentiated (indicated in green). Note, this technique does not give a full representation of the pore space present within this sample, as can be seen by the MIP data, which indicates the presence of pores with diameter smaller than 4 µm.*

properties for the Wilhelmøya Subgroup is shown in Fig. 12 including wireline logs, sedimentary textures and structures, net to gross sandstone-shale ratio, and litho-structural units. A subdivision of reservoir units based on reservoir properties is also presented. Cut-off criteria based on permeability values have not been used in this study due to the importance of fracture-enhanced permeability within sandstone beds. The net to gross sandstone-shale ratio of the more heterolithic reservoir unit 1 is estimated to vary between 0.3 and 0.6 and with a mean of approximately 0.5. The sequence-stratigraphic correlation in Fig. 12B indicates that reservoir unit 2 is laterally discontinuous and becomes truncated and eroded towards the west. In DH4, 5R and 7A, this reservoir zone has a net to gross ratio of 1. Reservoir zone 3 (Brentskardhaugen Bed) also varies in thickness but is characterised by a high net-to-gross ratio throughout the study area.

Porosity and permeability

The estimated burial depths, and more importantly the maximum burial temperature, imply that chemical compaction is the main factor responsible for the moderate porosities and low permeability measured in the Wilhelmøya Subgroup sandstones (Mørk, 2013). Detailed petrographic studies of sandstones from DH4 document considerable diagenetic impacts on the reservoir quality of the Wilhelmøya Subgroup. The sandstone data from DH4 also verify a distinct increase in mineralogical maturity compared to the underlying De Geerdalen Formation. The quartz-rich sandstones of the Wilhelmøya Subgroup also include a notable feldspar content and, as in the underlying De Geerdalen Formation, chert is the common rock fragment. Rounded, accessory grains of tourmaline and zircon support the earlier interpretations of sediment recycling. Variations in clay-mineral contents (up to 15%) in the bioturbated sandstones probably reflect both primary facies variations and diagenesis.

The diagenetic style of the quartz-rich sandstones includes quartz cementation associated with micro-stylolites, mineral dissolution and precipitation of pore-filling clay minerals, and commonly associated late pyrite and calcite. The chemical compaction resulted in major reductions of sandstone porosity and permeability. Permeability has been further reduced by a persistence of authigenic Fe-chlorite and fibrous illite in the pores, which explains the low matrix permeability values derived by conventional core plug measurements

The Slottet and Brentskardhaugen beds comprise phosphatic and non-phosphatic conglomerate beds as well as thin sandy interbeds. Thin-section study of the

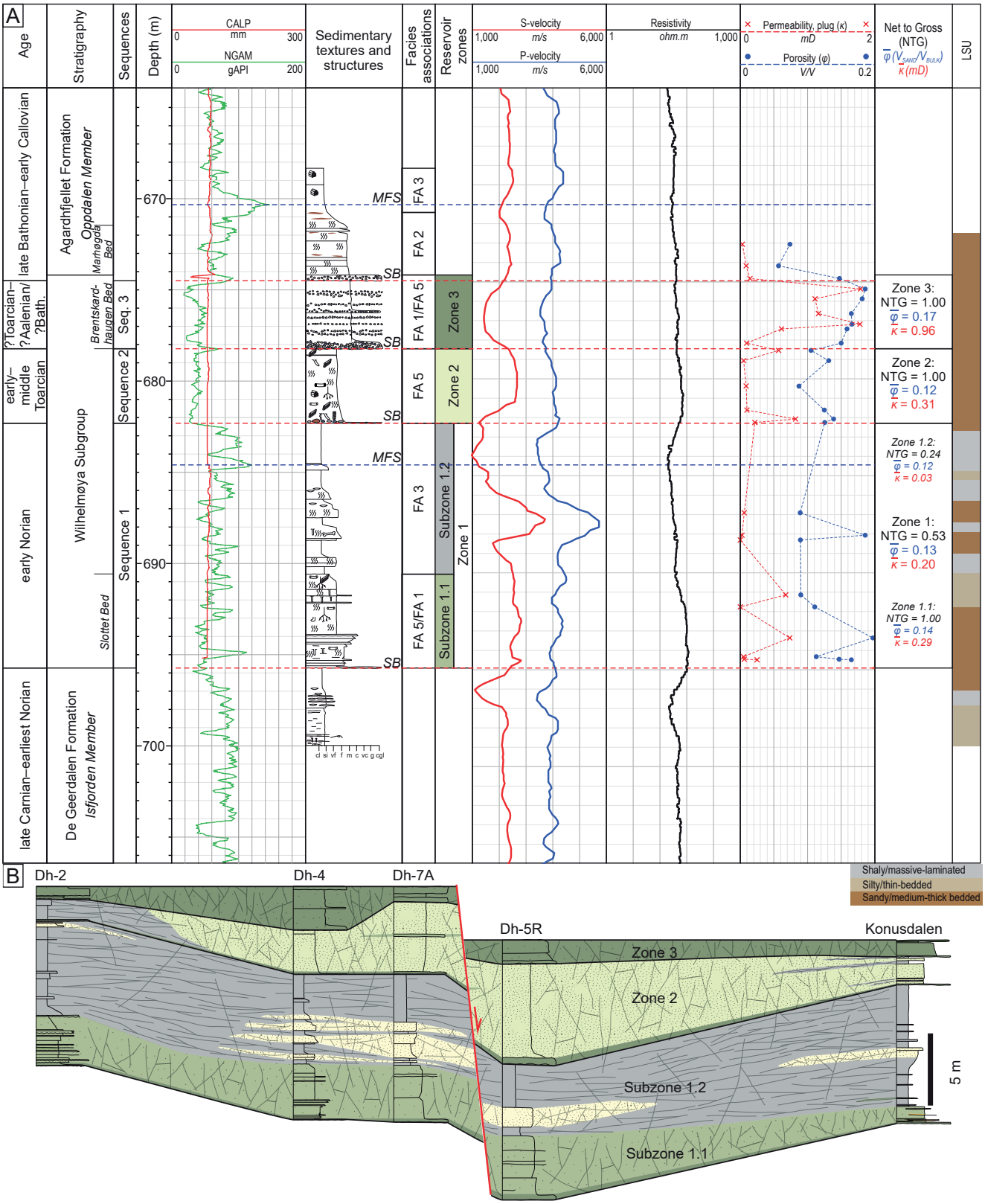
A
Age
Stratigraphy
Sequences
Depth (m)
CALP
mm
0
300
NGAM
gAPI
0
200
Sedimentary textures and structures
Facies associations
Reservoir zones
S-velocity
1,000
m/s
6,000
P-velocity
1,000
m/s
6,000
Resistivity
1
ohm.m
1,000
Permeability, plug (κ)
mD
0
2
Porosity (φ)
V/V
0
0.2
Net to Gross (NTG)
φ (V_SAND/V_BULK)
κ (mD)
LSU
late Bathonian–early Callovian
Agardhfjellet Formation
Oppdalen Member
Marnagda Bed
?Toarcian–?Aalenian/?Bath.
Brentskard-haugen Bed
Seq. 3
early–middle Toarcian
Sequence 2
Wilhelmøya Subgroup
early Norian
Sequence 1
Slottet Bed
late Carnian–earliest Norian
De Geerdalen Formation
Isfjorden Member
670
680
690
700
MFS
SB
FA 3
FA 2
FA 1/FA 5
FA 5
FA 5/FA 1
Zone 3
Zone 2
Subzone 1.2
Subzone 1.1
Zone 1
cl si vf f m c vc g cgl
Zone 3:
NTG = 1.00
φ = 0.17
κ = 0.96
Zone 2:
NTG = 1.00
φ = 0.12
κ = 0.31
Zone 1.2:
NTG = 0.24
φ = 0.12
κ = 0.03
Zone 1:
NTG = 0.53
φ = 0.13
κ = 0.20
Zone 1.1:
NTG = 1.00
φ = 0.14
κ = 0.29
B
Dh-2
Dh-4
Dh-7A
Dh-5R
Konusdalen
Shaly/massive-laminated
Silty/thin-bedded
Sandy/medium-thick bedded
Zone 3
Zone 2
Subzone 1.2
Subzone 1.1
5 m
FA1/5 LSU C
Good reservoir potential. Limited qtz cement
φ=0.15-0.20 (φ̄=0.17) κ=0.1-1.8 mD (κ̄=0.96 mD)
FA5/1 LSU C
Moderate reservoir potential. Limited qtz cement
φ=0.09-0.19 (φ̄=0.14) κ=0-0.7 mD (κ̄=0.29 mD)
FA5 LSU C
Moderate reservoir potential. Abundant qtz cement
φ=0.09-0.14 (φ̄=0.12) κ=0.05-0.8 mD (κ̄=0.31 mD)
FA3/4 LSU B
Very low reservoir potential. Abundant qtz cement
φ=0.09-0.19 (φ̄=0.12) κ=0-0.06 mD (κ̄=0.03 mD)
FA3/4 LSU A
No reservoir potential
Quartz cementation
LSU A
Shaly/massive-laminated. Dominated by low-angle fractures. Enhanced lateral connectivity
LSU B
Silty/thin-bedded. Both low- and high-angle fractures. Diffused/baffled vertical connectivity
LSU C
Sandy/medium-thick bedded. Dominated by high-angle fractures. Enhanced vertical connectivity

Figure 12. (A) Wireline logs and net-to-gross ratio (NTG), permeability and porosity measurements from DH–4. The wireline log suite includes caliper (CALP), natural gamma-ray (NGAM), sonic (S and P wave velocity) and resistivity. Litho-structural units (Ogata et al., 2012, 2014) also shown. Porosity and permeability values from Farokhpoor et al. (2010) and Magnabosco et al. (2014). Abbreviations: SB – sequence boundary, MFS – maximum flooding surface, FA – facies association. (B) Schematic illustration of the distribution of different reservoir zones in the Wilhelmøya Subgroup in and around the CO_2 storage area. A fault of approx. 5 m displacement is shown offsetting the reservoir between DH7A and DH5R. Diagenetic data from Mørk (2013) and litho-structural units (LSU) and natural fracture data from Ogata et al. (2012, 2014). Facies numbers correspond to those given in Rismyhr et al. (in press). Distance between sections is not to scale.

granule fraction and sandy matrix in DH4 shows an abundance of quartz (mono- and polygranular), chert fragments, minor K-feldspar, as well as reworked basinal grains of phosphate, glauconite and coated grains. Diagenesis has resulted in replacement of glauconite by chlorite and illite aggregates, and cementation of clay and phosphate matrix by microcrystalline siderite, whereas quartz cementation is relatively limited and only patchy within the sand-supported conglomerates (Mørk, 2013).

Permeability and porosity measurements from conventional core plug analysis were presented in Farokhpoor et al. (2010, 2013) and discussed in Mørk (2013). Permeability and porosity values have also been correlated with measurements derived from portable miniperm equipment (TinyPerm II; Magnabosco et al., 2014). The porosity and permeability measurements of samples from well DH4 revealed the best reservoir quality with porosities up to 20% and permeability up to 1.8 mD in conglomerates and thin sandstone beds (Fig. 12A) in the Brentskardhaugen Bed. The conglomerates with highest values are characterised by the presence of a sandstone matrix, where quartz cementation is locally reduced due to chlorite coatings. Lower porosities in similar facies is caused by quartz cement. In contrast, the phosphatic conglomerates and sandstones associated with the Slottet and Brentskardhaugen beds are characterised by low porosity and permeability due to siderite- and phosphate-cemented clay matrices (Mørk, 2013).

Reservoir zones

Three reservoir zones which correspond to the sequences defined by Rismyhr et al. (in press) are distinguished in the Wilhelmøya Subgroup (zones 1–3; Fig. 12B). The best injection and storage potential of the reservoir zones (best porosity and permeabilities) are found in reservoir zone 3, with an NTG ratio essentially equal to 1 and lateral continuity throughout the study area. Porosities of 15–20% (average 17%) and permeabilities of 0.1–1.8 mD (average 0.96 mD) are measured. The presence of clay-mineral coatings have inhibited extensive quartz cementation (Mørk, 2013) thereby preserving the relatively good reservoir properties. The contribution of fractures to reservoir potential must also be considered, and the reservoir zones can be correlated to lithostructural units (LSU) defined by Ogata et al. (2014) which show fracture characteristics as a function of the mechanical properties of the stratigraphy, i.e., LSU A (shaly/massive-laminated) is dominated by low-angle fractures and is observed within mudstone intervals, LSU B (silty/thin-bedded) includes a mix of both low- and high-angle fractures and is represented by thin sandstones, and LSU C (sandy/medium-thick bedded) that includes both low- and high-angle fractures present in medium-bedded sandstones.

Accordingly, reservoir zone 3 is considered to be the best reservoir zone in the Wilhelmøya Subgroup; however, zones with less favourable properties will contribute more to the storage space of the reservoir given their larger bulk volume. Reservoir zone 3 correlates approximately to LSU C (Fig. 12A; Ogata et al., 2014). Reservoir subzone 1.1 and zone 2 are considered to have moderate reservoir potential with NTG ratios up to 1, porosities of 9–19.6% (average 14%) and 8.7–13.9% (average 12%), and permeabilities of 0–0.73 mD (average 0.29 mD) and 0.05–0.82 mD (average 0.31 mD), respectively. Both zones correlate to LSU C (Fig. 12A; Ogata et al., 2014). Quartz cement is limited in subzone 1.1 due the presence of siderite and phosphate cement. In contrast, reservoir zone 2 contains abundant quartz cement with a patchy distribution reflecting the pre-existing bioturbation pattern (Mørk, 2013). Reservoir subzone 1.1 is laterally continuous throughout the study area, whereas reservoir zone 2 thins both towards the north and west. It also becomes slightly more heterolithic towards the north and is replaced by mudstones towards the west suggesting reduced reservoir potential in these directions. Reservoir subzone 1.2 is considered to have very little or no reservoir potential, consisting mainly of mudstones with a few thin and laterally restricted sandstones (NTG ratio 0.53 in DH–4). The porosities and permeabilities of these sandstones range from 9 to 18.7% and 0 to 0.06 mD, respectively, and the sandstones are extensively quartz cemented (Mørk, 2013). Reservoir subzone 1.2 correlates to LSU A and B (Fig. 12A; Ogata et al., 2014).

Discussion

The well pressure communication tests detailed herein show unequivocal support for the presence of vertical to sub-vertical heterogeneities within the Longyearbyen CO_2 target reservoir that act as baffles to fluid flow between DH5R and DH7A. Seismic imaging (two-dimensional) of the target reservoir intervals to date (Bælum et al., 2012) have failed to resolve the

heterogeneities responsible for this lack of pressure communication. In part, this could be explained by resolution limitations attributed to terrestrial seismic imaging of high-velocity rocks. Additionally, the presence of a 100–120 m-thick permafrost zone in Adventdalen (Johansen et al., 2003) likely contributes to imaging issues, (e.g., Matson et al., 2013). Permafrost raises the velocity of what would otherwise be weakly consolidated Quaternary cover. Natural arctic surface features (e.g., pingos), that represent local bodies of unfrozen sediment create low-velocity perturbations in the surrounding high-velocity permafrost. Abrupt lateral and vertical velocity variations detrimentally affect conventional surface seismic imaging of the reservoir.

In this section, vertical to sub-vertical geological heterogeneities are discussed with regard to how they may act as baffles to fluid flow. Three possible explanations for the observed lack of communication in well pressure communication tests are suggested, 1) Meso-scale normal faults formed during evolution of the WSFTB, 2) Cretaceous dolerite dykes emplaced in the Mesozoic successions during the HALIP event and 3) potential stratigraphic and/or diagenetic induced compartmentalisation. Further, the roll of fractures and impacts of the observed compartmentalisation are discussed with regard to potential CO_2 injection in the subsurface of Svalbard.

Faults as baffles

The widespread occurrence of subsurface baffling faults is consistent with outcrop and seismic observations throughout central Spitsbergen. The normal fault system affecting the reservoir outcrops in Konusdalen is therefore the most likely explanation for the lack of pressure communication between DH7A and DH5R during injection tests. Observations from outcrops (Fig. 6B) show sand-prone facies in the Wilhelmøya Subgroup are variably juxtaposed across faults. In the case of faults K2, K4 and K5, the sand-prone facies are self-separated across single fault planes, i.e., are juxtaposed against shaly-silty facies. These scenarios represent a high fault seal probability (P_{FS}) of between 0.7 and 1.0 (Færseth, 1996; Færseth et al., 2007). Faults K1 and K3 which contain several slip surfaces show partial across-fault self juxtaposition of sand-prone bodies, i.e., sand on sand contacts may allow for greater fluid communication across these fault zones. These scenarios represent lower P_{FS} values in the range of 0.3 and 0.6 (Færseth, 1996; Færseth et al., 2007). The faults that are antithetic to K5 show almost complete self juxtapostion of sand-prone facies across single slip surfaces, i.e., low P_{FS} values in the range of 0.0 and 0.3. For these latter examples with self juxtaposed sand-prone facies, and subsequent lower P_{FS} values, the consistent presence of clay abrasion membranes composed of between 35% and 65% clay minerals (Table 2) and an associated reduction in pore throat size in the fault rock can produce an effective seal (e.g., Freeman et al., 1998). For net to gross sandstone-shale ratios of 0.3 to 0.6, typical of sequence 1 in the Wilhelmøya Subgroup (Rismyhr et al., in press), calculation of shale-gouge ratios (SGR), i.e., the percentage of shale within a part of the sequence which has moved past a point on the fault surface, is of little benefit given that the values will be very high and our lack of control on the distribution of the faults in the subsurface. For a fault with a throw value of 3 m, SGR will equal 40 to 70% which would typically be interpreted as an effective fault seal (e.g., Knipe, 1992; Freeman et al., 1998).

In reality, however, it is hard to envisage faults of this scale acting as truly sealing structures. The immature nature of the structures (e.g., with throws no larger than 4 m) suggests faults are laterally discontinuous (Fig. 13A inset). Relay zones between adjacent faults may allow localised across-fault fluid transmissibility and subsequent communication between compartments (Walsh & Watterson, 1991; Cartwright et al., 1995; Childs et al., 1995; Meyer et al., 2002; Kristensen et al., 2008). In addition, the undulating nature of the fault gouge may result in gaps, i.e., sites of enhanced fluid transmissibility. The baffling capacity of such faults may be the net effect of a large number of these small structures and/or some contribution from other discontinuities such as igneous

Figure 13. *Schematic diagrams of the three, subseismic, geological heterogeneities potentially responsible for baffling fluid communication between DH7A (injection well) and DH5R (monitoring well). (A) Small-scale (less than 10 m displacement) faults as identified in the Konusdalen valley section. Faults affecting the reservoir section have considerable sealing capacity owing to the consistent presence of clay abrasion membranes in fault cores. Enhanced fluid flow both along strike and up-dip is also envisaged owing to high-intensity, fault parallel/subparallel fractures within the damage zones and presence of brecciation. Bottom left inlay: Fluid migration pathways may be preserved at relay zones between laterally discontinuous segments (Rotevatn et al., 2007). (B) Thin, less than 1 m-thick dykes as observed in outcrop at Botnehia and Hatten, may feed from a large sill seismically imaged at approx. 250 m below DH5R and DH7A. Numerous thin intrusions are also encountered within the Wilhelmøya Subgroup in DH4 but are likely sills (Ogata et al., 2014). The baffling capacity of dykes results from contact metamorphism where the reservoir country rock has undergone reductions in porosity and permeability. Similar to the faults, enhanced fluid flow is envisaged both up-dip and along-strike of the intrusion owing to intense, emplacement-related fractures striking parallel/subparallel to the intrusion. Across dyke, fluid transmission may, however, be facilitated by intrusion perpendicular cooling joints. (C) Minor stratigraphic pinch-outs may be facilitated by depositional geometries and diagenetic processes, although they are unlikely to explain the complete lack of communication between DH7A and DH5R.*

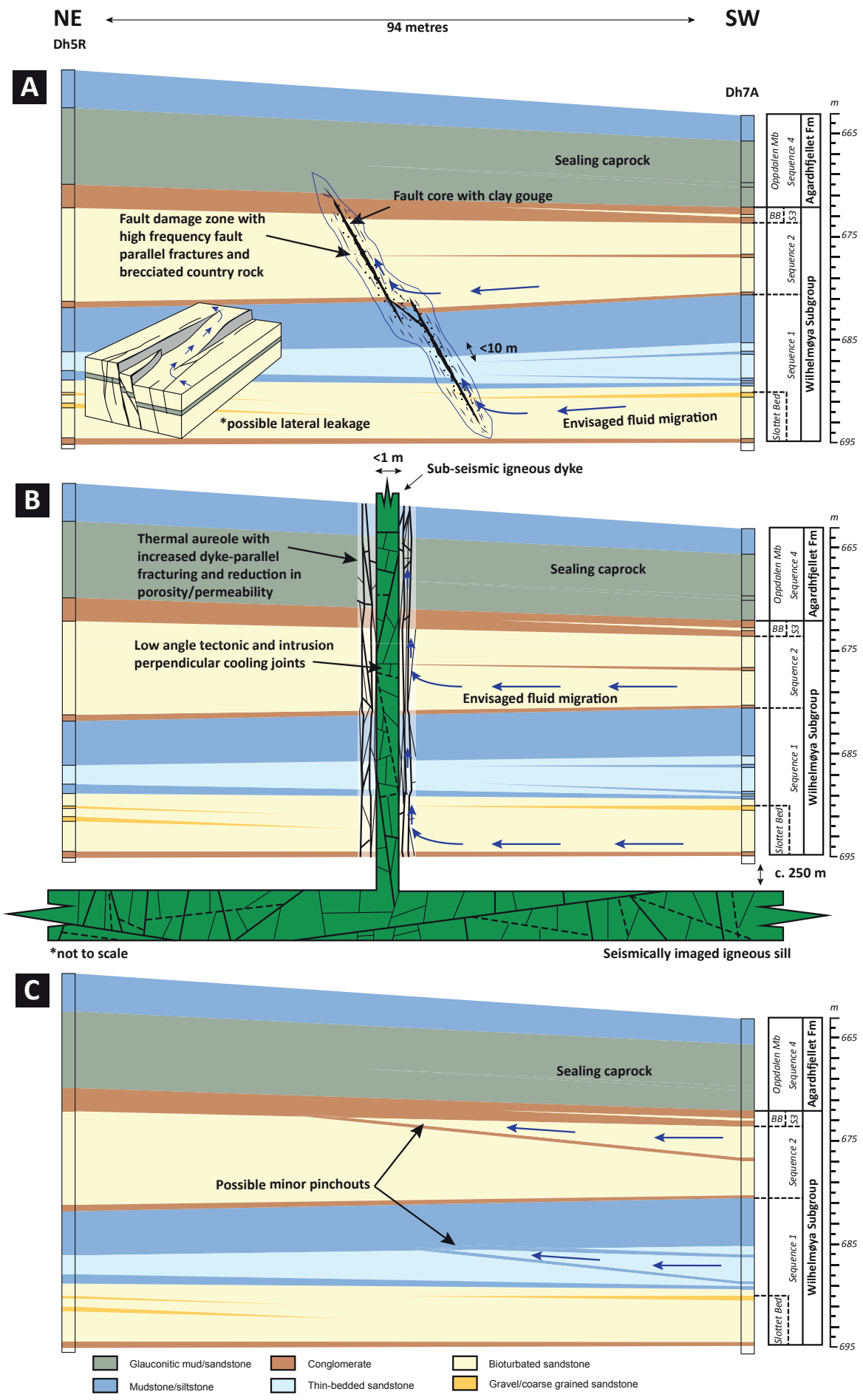
NE
94 metres
SW
Dh5R
A
Dh7A
Sealing caprock
Fault core with clay gouge
Fault damage zone with high frequency fault parallel fractures and brecciated country rock
<10 m
*possible lateral leakage
Envisaged fluid migration
<1 m
Sub-seismic igneous dyke
B
Thermal aureole with increased dyke-parallel fracturing and reduction in porosity/permeability
Low angle tectonic and intrusion perpendicular cooling joints
Sealing caprock
Envisaged fluid migration
c. 250 m
*not to scale
Seismically imaged igneous sill
C
Sealing caprock
Possible minor pinchouts
Oppdalen Mb
Sequence 4
Agardhfjellet Fm
BB
S3
Sequence 2
Sequence 1
Wilhelmøya Subgroup
Slottet Bed
m
665
675
685
695
Glauconitic mud/sandstone
Mudstone/siltstone
Conglomerate
Thin-bedded sandstone
Bioturbated sandstone
Gravel/coarse grained sandstone

bodies or stratigraphic pinchouts. While the faults likely impede flow of injected fluids, Huq et al. (2017) showed that the strontium isotope composition of formation water within the reservoir is uniform, suggesting these faults will not compartmentalise the reservoir on a geological time scale.

The presence of extensional faults in the otherwise compressional regime of the WSFTB is also somewhat anomalous. These normal faults have been related to the latest evolutionary phase of the WSFTB where, in the western hinterland, the elevated fold complex began to collapse resulting in extension along NNE-SSW- to NW-SE-striking normal faults, parallel with the earlier thrusting (Braathen et al., 1995). Ogata et al. (2012) relates local extension towards the foreland, i.e., the Konusdalen and Criocerasdalen faults described herein, to differential tectonic loading and perturbations of the compressional regime along strike of the WSFTB, where extensional faults parallel to the direction of thrusting accommodate thrust transport-normal extension.

The varying styles characterising the faults affecting the caprock and reservoir sections, i.e., the former exhibiting wider spacing, lower angles and anticlockwise strikes to the latter (Fig. 8), are credited to geomechanical variations (see above). Similar discrepancies in fracture trends across this boundary are also observed by Ogata et al. (2014). The transition also correlates stratigraphically with variations in fracture pressures identified in well tests. Mechanical laboratory testing and interpretation of injection test results by Bohloli et al. (2014) conclude that fracture pressure has a higher magnitude and gradient in the overburden than in the reservoir. In addition, in situ stresses in both successions vary, which has been used to speculate on potential fracture opening modes.

Igneous bodies as baffles

In terms of implications on reservoir properties, the emplacement of extensive igneous complexes has the potential to compartmentalise a reservoir by forming baffles/barriers to fluid flow (e.g., Gurba & Weber, 2001; Thomaz Filho et al., 2008), as well as introducing high-permeability fluid-flow pathways (e.g., Smit, 1978; Morel & Wikramaratna, 1982; Babiker & Gudmundsson, 2004; Sankaran et al., 2005; Mège & Rango, 2010; Senger et al., 2017). In some cases, individual intrusions can act as both conduits and baffles (e.g., Stearns, 1942; Rateau et al., 2013). The matrix of crystalline igneous rocks is typically tight, with submilliDarcy permeability and primary porosity commonly less than 0.5–1% (Van Wyk, 1963; Petford, 2003; Sruoga et al., 2004). Permeability within and adjacent to intrusions is dependent on the associated fracture networks typically generated by magma cooling, thermal contraction, magma emplacement and mechanical disturbance of the host rock (Senger et al., 2015b). Fracturing may be locally enhanced along intrusion–host rock interfaces, at dyke–sill junctions, or at the base of curving sills, thereby potentially enhancing permeability associated with these features.

Both Ogata et al. (2014) and Senger et al. (2014a) have shown that emplacement of the Diabasodden Suite caused local geochemical and mechanical perturbations to the sedimentary succession that influenced rock properties, including porosity and permeability. A thermal aureole encompassing the sill encountered towards the base of DH4 is observed and measures 160–195% of the physical sill thickness (Senger et al., 2014a). The aureole is characterised by hard, flint-like bleaching of the country rock where total organic carbon (TOC) decreases systematically towards the intrusion contacts. Increased fracturing within and around the intrusion, including some calcite-filled fractures, compared to background fracturing of the host rock indicates enhanced past fluid flow within and around the intrusions. Many of the fractures within the dolerites are thought to be related to natural cooling phenomena, i.e., cooling joints, while enhanced fracturing in the sedimentary host rock in the vicinity of the intrusion may be related to syn-emplacement mechanical deformation and later localised tectonic deformation due to mechanical contrasts, primarily during Palaeogene transpression. Moreover, incremental structural measurements by Senger et al. (2013) along the 4 km Deltaneset to Hatten beach sections (locations in Fig. 2), show considerable localised undulation in bedding attitude with a distinct deviation from the southwesterly regional dip (towards a northeasterly dip). Locally, adjacent to igneous intrusions, beds dip in excess of 20 degrees, likely the result of forced folding (e.g., Jackson et al., 2013) during emplacement of the igneous bodies.

Further evidence for enhanced fluid flow around the intrusions is observed offshore by Senger et al. (2013) and Roy et al. (2014) who document pockmark alignment along dolerite ridges on the seafloor. It is suggested that fluids may be channelled along the base of sills to the surface.

With respect to crediting doleritic sills as the cause of vertical pressure compartments within the target CO_2 successions, Senger et al. (2014a) concede that given the localised nature of intrusion occurrence and their general deeper stratigraphic position than the bulk of the target succession, intrusions are unlikely to be the primary cause of pressure compartmentalisation. The reservoir underpressure is more likely bounded by lateral lithological contacts or possibly the presence of the WSFTB-related décollement located at the Agardhfjellet–Rurikfjellet Formation interface. Small dykes, however, as seen in Botneheia must be present in the vicinity of DH4 in order to feed the thin sills encountered in DH4. These features very likely perturb fluid flow and represent possible seal bypass systems (Cartwright et al., 2007) if the dyke is permeable to fluid flow.

Stratigraphic compartmentalisation

An additional geological scenario that may account for the observed lateral pressure compartmentalisation is the possible presence of stratigraphic compartments, i.e., a segregation of flow units due to depositional and diagenetic heterogeneities (e.g., Jolley et al., 2010). Stratigraphic heterogeneities comprise many baffling and trapping features in hydrocarbon-bearing basins worldwide, e.g., Devonian reservoirs of the Paradox Basin in southeast Utah (Baars & Stevenson, 1981) and offshore Indonesia, Nigeria and the Gulf of Mexico (Posamentier & Kolla, 2003). Stratigraphic compartmentalisation can result from primary processes, i.e., depositional processes/geometries and/or diagenesis, i.e., lenses and facies variations in siliciclastic rocks. Secondary processes that can cause stratigraphic compartmentalisation commonly result from some lithological anomaly or variation that developed after deposition and diagenesis of the reservoir rock, and are usually associated with unconformities.

The Norian to Bathonian Wilhelmøya Subgroup was deposited as a highly condensed unit (now approximately 25 m thick) in an open marine-dominated inner-shelf to shore-face environment (Bjærke & Dypvik, 1977; Wierzbowski et al., 1981; Mørk et al., 1982, 1999; Bäckström & Nagy, 1985; Maher et al., 1989; Krajewski, 1990; Krajewski, 2000a, 2000b; Nagy & Berge, 2008; Reolid et al., 2010; Mørk, 2013; Rismyhr et al., in press). This inferred depositional environment has the potential to introduce stratigraphic closures and pinchouts, i.e., sand bodies may be lenticular in shape up dip and/or along strike of the depositional slope. Stratigraphic control (Rismyhr et al., in press) on the reservoir is good owing to extensive analyses of the strata where they crop out in the Deltaneset to Hatten area, and is complemented by correlation with four of the Longyearbyen CO_2 Lab wells which penetrate the target reservoir (DH2, DH4, DH5R and DH7A).

Despite the Wilhelmøya Subgroup showing the best reservoir properties in the Kapp Toscana Group, Mørk (2013) interpreted a moderate porosity and low permeability (up to 20% and 1.8 mD, respectively) due to deep burial and resultant chemical/physical compaction during the evolution of the WSFTB. In addition, low permeability in quartz-rich sandstones is caused by patchy (re)distribution of quartz cement, pressure solution (e.g., microstylolites) and pore-filling clay minerals. Miniperm measurements (Magnabosco et al., 2014) also showed that sandstones and conglomerates in the Wilhelmøya Subgroup have the best matrix properties for storage of CO_2.

The attitude of the depositional facies is critical with regard to the formation of stratigraphic compartmentalisation. Regionally, the Svalbard archipelago shows a gentle, two to four degree stratigraphic dip to the south owing to HALIP-related uplift in the Early Cretaceous (Maher, 2001). Locally, this is perturbed by forced folding during the emplacement of dolerite sills (discussed above).

The two-dimensional seismic coverage of the Longyearbyen CO_2 well park (Bælum et al., 2012) shows subtle evidence for the presence of stratigraphic pinchout geometries. Ideally, the identification of such geometries requires three-dimensional seismic to properly delineate their orientation and extent, e.g., Levey et al. (1992). Nevertheless, seismic reflectors representative of Triassic strata (Bælum et al., 2012) show bifurcation of seismic reflectors approximately towards the southeast. Additionally, in outcrop data, a deltaic sandstone in Konusdalen exhibits a lenticular geometry.

Despite the presence of many of the conditions that are associated with stratigraphic compartmentalisation within the Longyearbyen CO_2 Lab target reservoir, Ogata et al. (2012, 2014) have shown that even the lowest porosity/permeability litho-mechanical units in the reservoir, i.e., massive to laminated, shale-dominated intervals and massive to thin, interbedded, heterogeneous, mixed silty-shaly-sandy facies are characterised by a dense network of systematic fracture sets. These fractures are both high- and low-angled, which would possibly compromise any stratigraphic baffle, at least locally.

With respect to the horizontal compartmentalisation in the Svalbard stratigraphic succession, i.e., the presence of underpressure in the Wilhelmøya Subgroup, Huq et al. (2017), using the strontium isotope composition of formation water, showed there is a distinct barrier to vertical communication within the DeGeerdalen Formation, corresponding to a thin but presumably laterally extensive (>1.5 km) lagoonal mudrock interval (Rismyhr et al., in press).

The role of fractures

The larger abundance of fractures in outcrop samples in comparison to core samples is credited by Ogata et al. (2012) and Van Stappen et al. (2014, 2018) to the effects of unroofing, and subsequent decompaction that leads to reworking of pre-existing fractures. Furthermore, fracture abundance can be accentuated by the effects of freeze-thaw cycles (Tharp, 1987), i.e., frost wedging, which is caused by the repeated freeze-thaw cycle of water in extreme climates and consistent with the recent high latitudes of the Svalbard archipelago. Longer fracture lengths found in outcrop samples, in comparison with core samples have been credited to the same mechanisms. Fracture apertures are consistent between outcrop and core samples, mostly ranging between 123 and 283 μm, with a further population of microfractures showing apertures of approx. 25 μm being recognised in high-

resolution analysis (Van Stappen et al., 2014). These micro-fractures show preferential horizontal orientations as they exploit boundaries between sandstone sections and the interbedded claystones, whereas the larger fractures observed in outcrop are preferentially tectonically and uplift induced vertical fracturing and jointing, and are envisaged by Ogata et al. (2012, 2014) to facilitate preferential vertical and along-fault fluid migration. The discrepancy between the absolute values of the measured fracture apertures for field and drillcore samples is probably linked to the method used to calculate the maximum aperture (Brabant et al., 2011), i.e., from the micro-CT scans, which is linked to the scan resolution.

Given the severe under pressure of the target formation, the fractures are prone to open when subjected to relatively small pressure increments (Ogata et al., 2012). The primary function of the fracture systems in the target formationis to facilitate permeability. In addition, Senger et al. (2015a) estimated that 2.5% of storage resources are facilitated by the fracture network, which could increase if fractures open during injection.

Fractures induced during well tests (section 4.1) are likely the product of new large dimension fractures as evident by the test data (Fig. 12). It is probable, however, that some of these large-dimension fractures may result from opening and propagation of pre-existing natural fractures where they are preferentially orientated with regard to the injection-related stresses.

Towards injecting CO_2 in the Wilhelmøya Subgroup

The Wilhelmøya Subgroup can be considered an 'unconventional reservoir', given that it has low–moderate matrix porosity, significant fracture contribution to the pore volume, an abnormal pressure regime, compartmentalisation and a shallow storage depth (affecting the gas phase).

Senger et al. (2015a) presented a first-order static storage capacity assessment of the entire Kapp Toscana Group, with its 'upper' zone corresponding to the Wilhelmøya Subgroup. The subgroup exhibits the best reservoir properties of the Kapp Toscana Group but its limited thickness means that the Wilhelmøya Subgroup only contributes with 15.2% of the overall storage capacity. Significant uncertainty in input parameters was accounted for by stochastic Monte Carlo modelling using probabilistic distributions, and a scenario-based approach was implemented based primarily on the area accessible for drilling. Calculated storage capacity was matched to required volumes given 20 years of energy production from the coal-fueled power plant (1.2 million tons of CO_2 in total). The deterministic backward volumetric calculation presented by Senger et al. (2015a) indicates that CO_2 would occupy an area of 58 km^2 if only the Wilhelmøya Subgroup contributed as a reservoir and pressure would be adequate to maintain high-density CO_2. The main uncertainty is related to both the accessible area and the phase of CO_2 (liquid, supercritical vs. gas-phase) which is directly linked to the spatio-temporal evolution of the underpressured compartment.

The present results suggest that significant and subseismic reservoir compartmentalisation is present within the Wilhelmøya Sugroup. As such, accessing adequate storage capacity for CO_2 storage would likely require several wells and perhaps even horizontal wells capable of accessing numerous compartments. Fig. 14 presents a simple model for the position and orientation of heterogeneities responsible for the lack of pressure communication within the Wilhelmøya Subgroup. A subseismic fault, or array of faults, is envisaged to strike ENE–WSW approx. 40–60 m north of DH7A. This orientation is inferred from the faults observed in equivalent outcrops. Additional faults(s) may be located north of DH4.

Subsurface heterogeneities can increase sequestration capacity, i.e., the volume fraction of the subsurface available for CO_2 storage (Hovorka et al., 2004). In homogeneous reservoirs, CO_2 flow paths are controlled by buoyancy (assuming low viscosity of CO_2; see below) and, as such, usually only exploit upper reservoir levels. Heterogeneous rocks force CO_2 to exploit more dispersive flow paths resulting in a larger contact percentage and thereby increasing sequestration capacity. Furthermore, in a heterogeneous reservoir (with horizontal stratification), a larger distribution of stored CO_2 may decrease leakage risk by shortening the continuous column of buoyant gas acting on a capillary seal and inhibiting seal failure.

The phase in which CO_2 exists is a function of pressure and temperature conditions (Goos et al., 2011; Miri et al., 2014). To date, CO_2 storage has mostly been conducted at depths exceeding 800 m (White et al., 2004; Whittaker et al., 2004; Förster et al., 2006; Xue et al., 2006; Daley et al., 2008; Doughty et al., 2008; Vasco et al., 2008; Aradóttir et al., 2011; Eiken et al., 2011), where CO_2 naturally occurs as a supercritical fluid. The temperature gradient in the Longyearbyen target reservoir varies on average between 25 and 50°C/km below the water level at 225 m depth (Elvebakk, 2010; Senger et al., 2013). A maximum temperature of 31.8°C measured at 900 m depth (Elvebakk, 2010) lies just above the CO_2 critical point of 30.97°C (Goos et al., 2011). CO_2 is then likely to be in gas phase in this pilot study and exhibit a low viscosity (Senger et al., 2015a), unless pressure is built up by water injection prior to CO_2 injection. Flow barriers, however, such as faults, increase induced pressures considerably, and may perturb local conditions within the reservoir, leading to pockets of supercritical fluid (Chadwick et al., 2009). It would be of benefit to repeat some well injection tests using CO_2 in different phases; however, owing to the remote location of the pilot study, and the difficulty

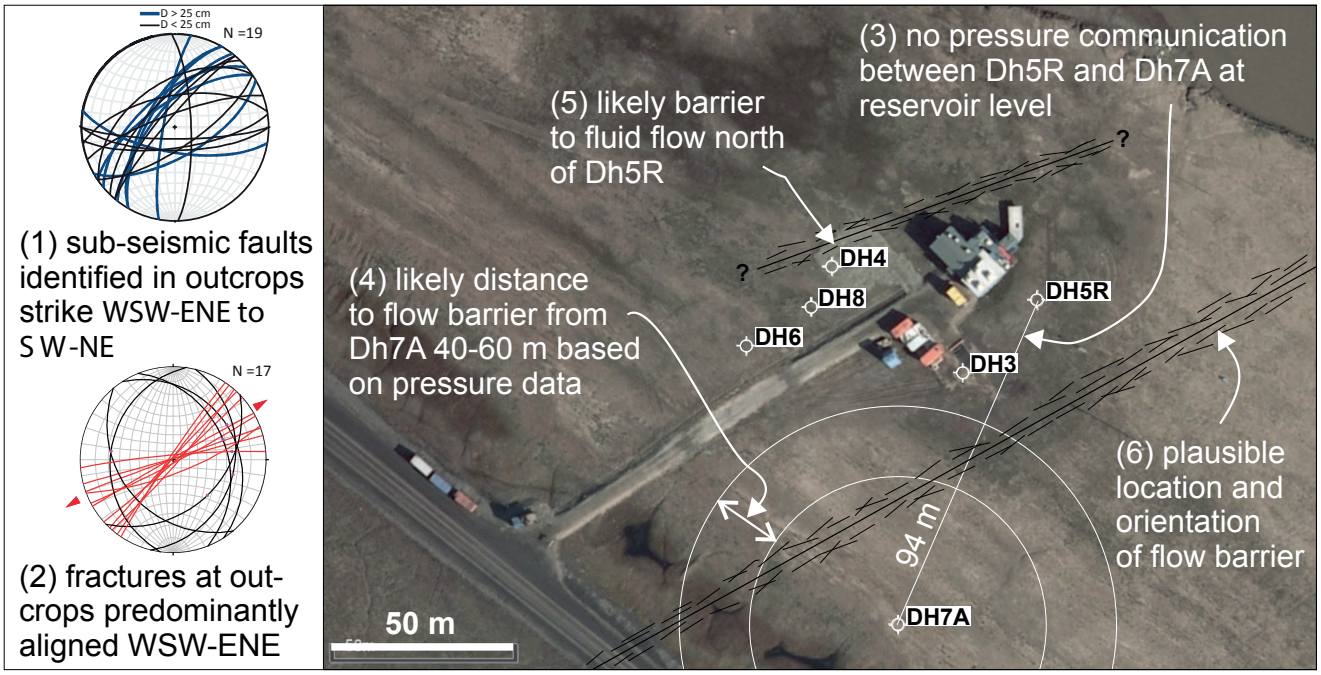

Figure 14. Summary of conclusive observations related to fracture-related fluid flow in the Wilhelmøya Subgroup at the Longyearbyen CO_2 lab drill site. Base satellite image courtesy of Norwegian Polar Institute.

to source CO_2, this has proven logistically challenging to date (Snorre Olaussen, UNIS CO_2 LAB Project Leader, pers. comm., 2017).

Conclusions

Well pressure tests, core- and outcrop-based analyses of discontinuities within a potential CO_2 storage unit on Svalbard have provided insight into the behaviour of injected fluids.

- The Wilhelmøya Subgroup represents a viable CO_2 storage reservoir with confirmed storage capacity and injectivity.
- The lack of interference during water injection tests in an observation well (DH5R) show limited lateral pressure communication within the reservoir, and the presence of barriers to flow or severe flow restriction within a relatively short distance (40–60 m) to the injector (DH7A). An additional barrier to fluid flow is predicted north of DH5R.
- An extensive natural fracture network contributes both to fluid injectivity and to storage potential. Micro-CT analysis provides reservoir information at the pore scale and allows for a quantification of fracture apertures. Field measurements indicate a potential for enhanced fracture-related fluid flow, primarily in a WSW–ENE trend, with a subordinate NNW–SSE trend.
- Large hydraulic fractures have been induced during the water injection tests, and have been modelled to obtain a satisfactory history match to the injection data. The fractures may be partially credited to pre-existing natural fractures that were preferentially orientated and propagated beyond their existing dimensions.
- Natural fractures contribute significantly to fluid injectivity in the Wilhelmøya Subgroup, although play a more substantial role in the De Geerdalen Formation where matrix porosity and permeability is worse.
- Analysis of petrographic diagenesis and paleo-temperature data shows that chemical compaction had major impact on reservoir quality.
- We propose that an extensional fault system consisting of relatively small (i.e., subseismic) but numerous segments is located between DH5R and DH7A, and oriented WSW–ENE in accordance with analogue fault systems identified in outcrop. Dolerite dykes and stratigraphic closures may also contribute to lateral pressure compartmentalisation.

Acknowledgments. We thank the industry partners in the Longyearbyen CO_2 Lab for their enthusiasm, technical advice and financial contributions: ConocoPhillips, Equinor, Store Norske Spitsbergen Kulkompani, Statkraft, Lundin Norway, Baker Hughes and Leonhard Nilsen & Sønner (http://co2-ccs.unis.no). We are also grateful for the

financial support given by the CLIMIT-program administered by the Research Council of Norway and supported by Gassnova. Field campaigns for M.M. and K.S. were supported by Arctic Field Grants from the Svalbard Science Forum. Schlumberger generously provided academic licenses for Petrel to UNIS. Beyene Girma Haile is thanked for processing samples for clay gouge analysis at the University of Oslo. Inger Laursen and Ola Eiken are thanked for their comments and suggestions which helped improve the clarity of the manuscript. The work is related to the Geological Input to Carbon Storage and Trias North projects (Research Council of Norway award numbers 200006 and 234152, respectively).

References

Abay, T.B., Karlsen, D.A., Lerch, B., Olaussen, S., Pedersen, J.H. & Backer-Owe, K. 2017: Migrated petroleum in outcropping Mesozoic sedimentary rocks in Spitsbergen: Organic geochemical characterization and implications for regional exploration. *Journal of Petroleum Geology 40*, 5–36. https://doi.org/10.1111/jpg.12662.

Andresen, A., Agyei-Dwarko, N.Y., Kristoffersen, M. & Hanken, N.M. 2014: A Timanian foreland basin setting for the late Neoproterozoic–Early Palaeozoic cover sequences (Dividal Group) of northeastern Baltica. *Geological Society of London Special Publications 390*, 157–175. https://doi.org/10.1144/SP390.29.

Anell, I., Braathen, A. & Olaussen, S. 2014: The Triassic-Early Jurassic of the northern Barents shelf: A regional understanding of the Longyearbyen CO_2 reservoir. *Norsk Geologisk Tidsskrift 94*, 83–98.

Aradóttir, E.S.P., Sigurdardóttir, H., Sigfússon, B. & Gunnlaugsson, E. 2011: CarbFix: a CCS pilot project imitating and accelerating natural CO_2 sequestration. *Greenhouse Gases: Science and Technology 1*, 105–118. https://doi.org/10.1002/ghg.18.

Árkai, P., Ferreiro Mählmann, R., Suchý, V., Balogh, K., Sýkorová, I. & Frey, M. 2002: Possible effects of tectonic shear strain on phyllosilicates: A case study from the Kandersteg area, Helvetic domain, Central Alps, Switzerland. *Schweizerische Mineralogische Und Petrographische Mitteilungen 82*, 273–290. https://doi.org/10.5169/seals-62365.

Baars, D.L. & Stevenson, G.M. 1981: Subtle Stratigraphic Traps in Paleozoic Rocks of Paradox Basin. *American Association of Petroleum Geologists Bulletin, 65*, 892–893. https://doi.org/10.1306/2F919B75-16CE-11D7-8645000102C1865D.

Babiker, M. & Gudmundsson, A. 2004: The effects of dykes and faults on groundwater flow in an arid land: the Red Sea Hills, Sudan. *Journal of Hydrology 297*, 256–273. https://doi.org/10.1016/j.jhydrol.2004.04.018.

Bachu, S. 2008: CO_2 storage in geological media: role, means, status and barriers to deployment. *Progress in Energy and Combustion Science 34*, 254–273. https://doi.org/10.1016/j.pecs.2007.10.001.

Bäckström, S.A. & Nagy, J. 1985: *Depositional history and fauna of a Jurassic phosphorite conglomerate (the Brentskardhaugen Bed) in Spitsbergen*. Skrifter 183, Norsk Polarinstitutt, Oslo, 5–41.

Beliveau, D., Payne, D. & Mundry, M. 1993: Waterflood and CO_2 Flood of the Fractured Midale Field (includes associated paper 22947). *Journal of Petroleum Technology 45*, 881–887. https://doi.org/10.2118/22946-PA.

Benson, S.M. & Cole, D.R. 2008: CO_2 sequestration in deep sedimentary formations. *Elements 4*, 325–331. https://doi.org/10.2113/gselements.4.5.325.

Bergh, S.G., Braathen, A. & Andresen, A. 1997: Interaction of basement-involved and thin-skinned tectonism in the Tertiary fold-thrust belt of central Spitsbergen, Svalbard. *American Association of Petroleum Geologists Bulletin 81*, 637–661. https://doi.org/10.1306/522B43F7-1727-11D7-8645000102C1865D.

Birol, F. 2010: World energy outlook 2010.*International Energy Agency*, https://www.iea.org/publications/freepublications/publication/weo2010.pdf.

Bjærke, T. & Dypvik, H. 1977: Quaternary "stromatolitic" limestone of subglacial origin from Scandinavia. *Journal of Sedimentary Research 47*, 1321–1327. https://doi.org/10.1306/212F7333-2B24-11D7-8648000102C1865D.

Blinova, M., Faleide, J.I., Gabrielsen, R.H. & Mjelde, R. 2012: Seafloor expression and shallow structure of a fold-and-thrust system, Isfjorden, west Spitsbergen. *Polar Research 31*, 1–13. https://doi.org/10.3402/polar.v31i0.11209.

Bohloli, B., Skurtveit, E., Grande, L., Titlestad, G.O., Børresen, M.H., Johnsen, Ø. & Braathen, A. 2014: Evaluation of reservoir and caprock integrity for the longyearbyen CO_2 storage pilot based on laboratory experiments and injection tests. *Norsk Geologisk Tidsskrift 94*, 171–187.

Boles, J.R. & Franks, S.G. 1979: Clay diagenesis in Wilcox sandstones of southwest Texas: implications of smectite diagenesis on sandstone cementation. *Journal of Sedimentary Research 49*, 55–70.

Braathen, A. & Bergh, S.G. 1995: Kinematics of Tertiary deformation in the basement-involved fold-thrust complex, western Nordenskiøld Land, Svalbard: tectonic implications based on fault-slip data analysis. *Tectonophysics 249*, 1–29. https://doi.org/10.1016/0040-1951(95)00036-M.

Braathen, A., Bergh, S.G. & Maher, H.D. 1995: Structural outline of a Tertiary Basement-cored uplift/inversion structure in western Spitsbergen, Svalbard: Kinematics and controlling factors. *Tectonics 14*, 95–119. https://doi.org/10.1029/94TC01677.

Braathen, A., Bergh, S.G., Karlsen, F., Maher, H.D.J., Andresen, A., Hansen, A.I. & Bergvik, A. 1999: Kinematics of the Isfjorden-Ymerbukta Fault Zone: a dextral oblique-thrust ramp in the Tertiary fold-thrust belt of Spitsbergen. *Norsk Geologisk Tidsskrift 79*, 228–239. https://doi.org/10.1080/002919699433681.

Braathen, A., Nordgulen, O., Osmundsen, P.T., Andersen, T.B., Solli, A. & Roberts, D. 2000: Devonian, orogen-parallel, opposed extension in the Central Norwegian Caledonides. *Geology 28*, 615–618. https://doi.org/10.1130/0091-7613(2000)28<615:DOOEIT>2.0.CO;2.

Braathen, A., Osmundsen, P.T. & Gabrielsen, R.H. 2004: Dynamic development of fault rocks in a crustal-scale detachment: An example from western Norway. *Tectonics 23*, 1–21. https://doi.org/10.1029/2003TC001558.

Braathen, A., Tveranger, J., Fossen, H., Skar, T., Cardozo, N., Semshaug, S.E., Bastesen, E. & Sverdrup, E. 2009. Fault facies and its application to sandstone reservoirs. *American Association of Petroleum Geologists Bulletin 93*, 891–917. https://doi.org/10.1306/03230908116.

Braathen, A., Bælum, K., Maher, H. & Buckley, S.J. 2011: Growth of extensional faults and folds during deposition of an evaporite-dominated half-graben basin; the Carboniferous Billefjorden Trough, Svalbard. *Norsk Geologisk Tidsskrift 91*, 137–161.

Braathen, A., Bælum, K., Christiansen, H.H., Dahl, T., Eiken, O., Elvebakk, H. & Vagle, K. 2012: The Longyearbyen CO2 Lab of Svalbard, Norway — initial assessment of the geological conditions for CO_2 sequestration. *Norwegian Journal of Geology 92*, 353–376.

Braathen, A., Osmundsen, P.T., Maher, H. & Ganerød, M. 2018: The Keisarhjelmen detachment records Silurian–Devonian extensional collapse in Northern Svalbard. *Terra Nova 30*, 34–39. https://doi.org/10.1111/ter.12305.

Brabant, L., Vlassenbroeck, J., De Witte, Y., Cnudde, V., Boone, M.N., Dewanckele, J. & Van Hoorebeke, L. 2011: Three-Dimensional Analysis of High-Resolution X-Ray Computed Tomography Data with Morpho+. *Microscopy and Microanalysis 17*, 252–263. https://doi.org/10.1017/S1431927610094389.

Buckley, S.J., Naumann, N., Kurz, T.H. & Eide, C.H. 2016: *2nd Virtual Geoscience Conference, Proceedings Volume*. Uni Research CIPR, Bergen, Norway, 212 pp.

Bælum, K., Johansen, T.A., Johnsen, H., Rød, K., Ruud, B.O. & Braathen, A. 2012: Subsurface structures of the longyearbyen CO_2 lab study area in central Spitsbergen (arctic Norway), as mapped by reflection seismic data. *Norsk Geologisk Tidsskrift 92*, 377–389.

Cartwright, J.A., Trudgill, B.D. & Mansfield, C.S. 1995: Fault growth by segment linkage: an explanation for scatter in maximum displacement and trace length data from the Canyonlands Grabens of SE Utah. *Journal of Structural Geology 17*, 1319–1326. https://doi.org/10.1016/0191-8141(95)00033-A.

Cartwright, J., Huuse, M. & Aplin, A. 2007: Seal bypass systems. *American Association of Petroleum Geologists Bulletin 91*, 1141–1166. https://doi.org/10.1306/04090705181.

Casciello, E., Cesarano, M. & Cosgrove, J.W. 2004: Shear deformation of pelitic rocks in a large-scale natural fault. *Geological Society of London Special Publications 224*, 113–125. https://doi.org/10.1144/GSL.SP.2004.224.01.08.

Chadwick, R.A., Noy, D., Arts, R. & Eiken, O. 2009: Energy Procedia Latest time-lapse seismic data from Sleipner yield new insights into CO_2 plume development. *Energy Procedia 1*, 2103–2110. https://doi.org/10.1016/j.egypro.2009.01.274.

Childs, C., Watterson, J. & Walsh, J.J. 1995: Fault overlap zones within developing normal fault systems. *Journal of the Geological Society 152*, 535–549. https://doi.org/10.1144/gsjgs.152.3.0535.

Cnudde, V. & Boone, M.N. 2013: High-resolution X-ray computed tomography in geosciences: A review of the current technology and applications. *Earth-Science Reviews 123*, 1–17. https://doi.org/10.1016/j.earscirev.2013.04.003.

Cnudde, V., Cwirzen, A., Masschaele, B. & Jacobs, P.J.S. 2009: Porosity and microstructure characterization of building stones and concretes. *Engineering Geology 103*, 76–83. https://doi.org/10.1016/j.enggeo.2008.06.014.

Corfu, F., Polteau, S., Planke, S., Faleide, J.I., Svensen, H., Zayoncheck, A. & Stolbov, N. 2013: U–Pb geochronology of Cretaceous magmatism on Svalbard and Franz Josef Land, Barents Sea Large Igneous Province. *Geological Magazine 150*, 1127–1135. https://doi.org/10.1017/S0016756813000162.

Cowie, P.A. & Scholz, C.H. 1992: Displacement-length scaling relationship for faults: data synthesis and discussion. *Journal of Structural Geology 14*, 1149–1156. https://doi.org/10.1016/0191-8141(92)90066-6.

Daley, T.M., Myer, L.R., Peterson, J.E., Majer, E.L. & Hoversten, G.M. 2008: Time-lapse crosswell seismic and VSP monitoring of injected CO_2 in a brine aquifer. *Environmental Geology 54*, 1657–1665. https://doi.org/10.1007/s00254-007-0943-z.

Dallmann, W.K. 1999: *Lithostratigraphic Lexicon of Svalbard: review and recommendations for nomenclature use: Upper Paleozoic to Quaternary Bedrock. Committee on the Stratigraphy of Svalbard*. Norsk Polarinstitutt, 318 pp.

Dallmann, W.K., Ohta, Y., Elvevold, S. & Blomeier, D. 2002: Bedrock map of Svalbard and Jan Mayen, scale 1:750,000, *Norwegian polar institute*.

Dellisanti, F. & Valdrè, G. 2008: Linear relationship between thermo-dehydroxylation and induced-strain by mechanical processing in vacuum: The case of industrial kaolinite, talc and montmorillonite. *International Journal of Mineral Processing 88*, 94–99. https://doi.org/10.1016/j.minpro.2008.07.001.

Dellisanti, F., Pini, G.A. & Baudin, F. 2010: Use of T max as a thermal maturity indicator in orogenic successions and comparison with clay mineral evolution. *Clay Minerals 45*, 115–130. https://doi.org/10.1180/claymin.2010.045.1.115.

Dimakis, P., Braathen, B.I., Faleide, J.I., Elverhøi, A. & Gudlaugsson, S.T. 1998: Cenozoic erosion and the preglacial uplift of the Svalbard-Barents Sea region. *Tectonophysics 300*, 311–327. https://doi.org/10.1016/S0040-1951(98)00245-5.

Doughty, C., Freifeld, B.M. & Trautz, R.C. 2008: Site characterization for CO_2 geologic storage and vice versa: The Frio brine pilot, Texas, USA as a case study. *Environmental Geology 54*, 1635–1656. https://doi.org/10.1007/s00254-007-0942-0.

Dypvik, H., Nagy, J., Eikeland, T.A., Backer-Owe, K. & Johansen, H. 1991: Depositional conditions of the Bathonian to Hauterivian Janusfjellet Subgroup, Spitsbergen. *Sedimentary Geology 72*, 55–78. https://doi.org/10.1016/0037-0738(91)90123-U.

Eiken, O.L.A. & Austegard, A. 1987: The Tertiary orogenic belt of West-Spitsbergen: Seismic expressions of the offshore sedimentary basins, *Norsk Geologisk Tidsskrift 67*, 383–394.

Eiken, O., Ringrose, P., Hermanrud, C., Nazarian, B., Torp, T.A. & Høier, L. 2011: Lessons learned from 14 years of CCS operations: Sleipner, In Salah and Snøhvit. *Energy Procedia 4*, 5541–5548. https://doi.org/10.1016/j.egypro.2011.02.541.

Elvebakk, H. 2010: Results of borehole logging in well LYB CO_2, Dh4 of 2009, Longyearbyen, Svalbard. *Norges geologiske undersøkelse Report 2010.018*, 35 pp.

Faleide, J.I., Vågnes, E. & Gudlaugsson, S.T. 1993: Late Mesozoic-Cenozoic evolution of the southwestern Barents Sea in a rift-shear tectonic setting. *Marine and Petroleum Geology 10*, 186–214. https://doi.org/10.1016/0264-8172(93)90104-Z.

Faleide, J.I., Tsikalas, F., Mjelde, R., Wilson, J. & Eldholm, O. 2008: Structure and evolution of the continental margin off Norway and the Barents Sea. *Episodes 31*, 82–91.

Farokhpoor, R., Torsæter, O., Baghbanbashi, T., Mørk, A. & Lindeberg, E. 2010: Experimental and Numerical Simulation of CO_2 Injection Into Upper-Triassic Sandstones in Svalbard, Norway. *Society of Petroleum Engineers*, SPE 139524, https://doi.org/10.2118/139524-MS.

Farokhpoor, R., Bjørkvik, B.J.A., Lindeberg, E. & Torsæter, O. 2013: CO_2 wettability behavior during CO_2 sequestration in saline aquifer-An Experimental study on minerals representing sandstone and carbonate. *Energy Procedia 37*, 5339–5351. https://doi.org/10.1016/j.egypro.2013.06.452.

Farokhpoor, R., Lindeberg, E.G.B., Torsæter, O., Mørk, M.B. & Mørk, A. 2014: Permeability and relative permeability measurements for CO_2-brine system at reservoir conditions in low permeable sandstones in Svalbard. Greenhouse Gases: *Science and Technology* 4, 36–52.

Förster, A., Norden, B., Zinck-Jørgensen, K., Frykman, P., Kulenkampff, J., Spangenberg, E. & Hurter, S. 2006: Baseline characterization of the CO_2 SINK geological storage site at Ketzin, Germany. *Environmental Geosciences 13*, 145–161. https://doi.org/10.1306/eg.02080605016.

Freeman, B., Yielding, G., Needham, D.T. & Badley, M.E. 1998: Fault seal prediction: the gouge ratio method. *Geological Society of London Special Publications 127*, 19–25. https://doi.org/10.1144/GSL.SP.1998.127.01.03.

Frey, M. 1987: *Low Temperature Metamorphism*. Blackie, New York, 351 pp.

Færseth, R.B. 1996: Interaction of Permo-Triassic and Jurassic extensional fault-blocks during the development of the northern North Sea. *Journal of the Geological Society 153*, 931–944. https://doi.org/10.1144/gsjgs.153.6.0931.

Færseth, R.B., Johnsen, E. & Sperrevik, S. 2007: Methodology for risking fault seal capacity: Implications of fault zone architecture. *American Association of Petroleum Geologists Bulletin 91*, 1231–1246. https://doi.org/10.1306/03080706051.

Gabrielsen, R.H. 1992: A structural outline of Forlandsundet Graben, Prins Karls Forland, Svalbard. *Norsk Geologisk Tidsskrift 72*, 105–120.

Gaina, C., Gernigon, L. & Ball, P. 2009: Palaeocene-Recent plate boundaries in the NE Atlantic and the formation of the Jan Mayen microcontinent. *Journal of the Geological Society 166*, 601–616. https://doi.org/10.1144/0016-76492008-112.

Gee, D.G., Bogolepova, O.K. & Lorenz, H. 2006: The Timanide, Caledonide and Uralide orogens in the Eurasian high Arctic, and relationships to the palaeo-continents Laurentia, Baltica and Siberia. *Geological Society of London Memoirs 32*, 507–520. https://doi.org/10.1144/GSL.MEM.2006.032.01.31.

Glørstad-Clark, E., Faleide, J.I., Lundschien, B.A. & Nystuen, J.P. 2010: Triassic seismic sequence stratigraphy and paleogeography of the western Barents Sea area. *Marine and Petroleum Geology 27*, 1448–1475. https://doi.org/10.1016/j.marpetgeo.2010.02.008.

Goss, A.L. 2013: *Analysis of brittle Paleogene structures in the Svea region, eastern Spitsbergen, Svalbard*. Bachelor's thesis, Bates College, Lewiston, Maine, 50 pp.

Goos, E., Riedel, U., Zhao, L. & Blum, L. 2011. Phase diagrams of CO_2 and CO_2 -N2 gas mixtures and their application in compression processes. *Energy Procedia 4*, 3778–3785. https://doi.org/10.1016/j.egypro.2011.02.312.

Gurba, L.W. & Weber, C.R. 2001: Effects of igneous intrusions on coalbed methane potential, Gunnedah Basin, Australia. *International Journal of Coal Geology 46*, 113–131. https://doi.org/10.1016/S0166-5162(01)00020-9.

Haile, B.G., Czarniecka, U., Xi, K., Smyrak-Sikora, A., Jahren, J., Braathen, A. & Hellevang, H. 2018: Hydrothermally induced diagenesis: Evidence from shallow marine-deltaic sediments, Wilhelmøya, Svalbard. *Geoscience Frontiers*. https://doi.org/10.1016/j.gsf.2018.02.015.

Harland, W.B. & Geddes, I. 1997: Triassic history (chapter 18). The Geology of Svalbard, *Geological Society Memoirs 17,* 340–362. https://doi.org/10.1144/GSL.MEM.1997.017.01.18.

Harland, W.B., Wallis, R.H. & Gayer, R.A. 1966: A revision of the lower Hecla Hoek succession in central north Spitsbergen and correlation elsewhere. *Geological Magazine 103*, 70–97. https://doi.org/10.1017/S0016756800050433.

Helland-Hansen, W. 2010: Facies and stacking patterns of shelf-deltas within the Palaeogene Battfjellet Formation, Nordenskiold Land, Svalbard: Implications for subsurface reservoir prediction. *Sedimentology 57*, 190–208. https://doi.org/10.1111/j.1365-3091.2009.01102.x.

Hovorka, S.D., Doughty, C., Benson, S.M., Pruess, K. & Knox, P.R. 2004: The impact of geological heterogeneity on CO_2 storage in brine formations: a case study from the Texas Gulf Coast. *Geological Society of London Special Publications 233*, 147–163. https://doi.org/10.1144/GSL.SP.2004.233.01.10.

Hower, J., Eslinger, E.V., Hower, M.E. & Perry, E.A. 1976: Mechanism of burial metamorphism of argillaceos sediment. *Geological Society of America Bulletin 87*, 725–737. https://doi.org/10.1130/0016-7606(1976)87<725:MOBMOA>2.0.CO;2.

Humlum, O., Instanes, A. & Sollid, J.L. 2003: Permafrost in Svalbard: A review of research history, climatic background and engineering challenges. *Polar Research 22*, 191–215. https://doi.org/10.1111/j.1751-8369.2003.tb00107.x.

Huq, F., Smalley, P.C., Mørkved, P.T., Johansen, I., Yarushina, V. & Johansen, H. 2017: The Longyearbyen CO 2 Lab: Fluid communication in reservoir and caprock. *International Journal of Greenhouse Gas Control 63*, 59–76. https://doi.org/10.1016/j.ijggc.2017.05.005.

Høy, T. & Lundschien, B.A. 2011: Triassic deltaic sequences in the northern Barents Sea (chapter 15). *Geological Society of London Memoirs 35*, 249–260. https://doi.org/10.1144/M35.15.

IEA 2008: Key world energy statistics. *International Energy Agency, Paris, France*, p. 82.

IPCC 2005: IPCC Special Report on Carbon Dioxide Capture and Storage. Prepared by Working Group III of the Intergovernmental Panel on Climate Change. *IPCC, Cambridge University Press, Cambridge, United Kingdom and New York, USA*, *4*, 442. https://www.ipcc.ch/pdf/special-reports/srccs/srccs_wholereport.pdf.

Jackson, C.A.L., Schofield, N. & Golenkov, B. 2013: Geometry and controls on the development of igneous sill–related forced folds: A 2-D seismic reflection case study from offshore southern Australia. *Geological Society of America Bulletin 125*, 1874–1890. https://doi.org/10.1130/B30833.1.

Johansen, T.A., Digranes, P., van Schaack, M. & Lønne, I. 2003: Seismic mapping and modeling of near-surface sediments in polar areas. *Geophysics 68*, 566–573. https://doi.org/10.1190/1.1567226.

Jolley, S.J., Fisher, Q.J. & Ainsworth, R.B. 2010: Reservoir compartmentalization: an introduction. *Geological Society of London Special Publications 347*, 1–8. https://doi.org/10.1144/SP347.1.

Klausen, T.G., Ryseth, A.E., Helland-Hansen, W., Gawthorpe, R. & Laursen, I. 2015: Regional development and sequence stratigraphy of the Middle to Late Triassic Snadd Formation, Norwegian Barents Sea. *Marine and Petroleum Geology 62*, 102–122. https://doi.org/10.1016/j.marpetgeo.2015.02.004.

Knarud, R. 1980: *A sedimentological and diagenetic survey of Cape Toscana formation sediments in Svalbard*. Cand. Real. thesis, University of Oslo, Department of Geosciences, 1–208.

Knipe, R.J. 1992: Faulting processes and fault seal. *Norwegian Petroleum Society Special Publications 1*, 325–342. https://doi.org/10.1016/B978-0-444-88607-1.50027-9.

Koevoets, M.J., Abay, T.B., Hammer, Ø. & Olaussen, S. 2016: High-resolution organic carbon-isotope stratigraphy of the Middle Jurassic-Lower Cretaceous Agardhfjellet Formation of central Spitsbergen, Svalbard. *Palaeogeography, Palaeoclimatology, Palaeoecology 449*, 266–274. https://doi.org/10.1016/j.palaeo.2016.02.029.

Koevoets, M.J., Hammer, Ø., Olaussen S., Senger K., Smelror M. 2018: Facies, bio- and sequence stratigraphy of the Middle Jurassic to Lower Cretaceous Agardhfjellet Formation in central Spitsbergen. *Norwegian Journal of Geology 98*. https://dx.doi.org/10.17850/njg98-4-01.

Krajewski, K. 1990: Phosphoritization in a starved shallow shelf environment: the Brentskardhaugen Bed (Toarcian-Bajocian) in Spitsbergen. *Polish Polar Research 2*, 331–344.

Krajewski, K.P. 2000a: Isotopic composition of apatite-bound sulphur in the Triassic phosphogenic facies in Svalbard. *Studia Geologica Polonica 116*, 85–109.

Krajewski, K.P. 2000b: Phosphorus concentration and organic carbon preservation in the Blanknuten Member (Botneheia Formation, Middle Triassic), Sassenfjorden, Spitsbergen. *Studia Geologica Polonica 116*, 139–173.

Kristensen, M.B., Childs, C.J. & Korstgård, J.A. 2008: The 3D geometry of small-scale relay zones between normal faults in soft sediments. *Journal of Structural Geology 30*, 257–272. https://doi.org/10.1016/j.jsg.2007.11.003.

Kubler, B. 1967: The crystallinity of the illite and the altogether superior zones of the metamorphism. *Symposium on Tectonic Floors, La Baconnière, Neuchâtel*, 105–122.

Larsen, L. 2010: Analyses of Injection and Falloff Data from DH4, Aug. 12 - Sept. 4, 2010. *Longyearbyen* CO_2 *Lab UNIS Report 2010–14*, 1–30.

Larsen, L. 2012: Analyses of Sept. 2011 Upper Zone Injection and Falloff Data from DH6 and Interference Data from DH5. *Longyearbyen CO_2 Lab UNIS Report 2012–8*.

Leever, K.A., Gabrielsen, R.H., Faleide, J.I. & Braathen, A. 2011: A transpressional origin for the West Spitsbergen fold-and-thrust belt: Insight from analog modeling. *Tectonics 30*, 1–24. https://doi.org/10.1029/2010TC002753.

Levey, R.A., Sippel, M.A., Finley, R.J. & Langford, R.P. 1992: Stratigraphic compartmentalization within gas reservoirs: Examples from fluvial-deltaic reservoirs of the Texas Gulf Coast. *South Texas Geological Society Bulletin 33*, 7–16.

Lord, G.S. 2013: *Steep Fracture Patterns and Their Characteristics Within The Triassic De Geerdalen Formation On Svalbard: An emphasis on regional trends, local variations and lithological controls*. MSc thesis, Norwegian University of Science and Technology, Department of Geology and Mineral Resources Engineering, 200 pp.

Magnabosco, C., Braathen, A. & Ogata, K. 2014. Permeability model of tight reservoir sandstones combining core-plug and miniperm analysis of drillcore; longyearbyen CO_2lab, Svalbard. *Norsk Geologisk Tidsskrift 94*, 189–200.

Maher Jr., H.D. 2001: Manifestations of the Cretaceous High Arctic Large Igneous Province in Svalbard. *The Journal of Geology 109*, 91–104. https://doi.org/10.1086/317960.

Maher Jr., H.D. & Braathen, A. 2011: Løvehovden fault and Billefjorden rift basin segmentation and development, Spitsbergen, Norway. *Geological Magazine 148*, 154–170. https://doi.org/10.1017/S0016756810000567.

Maher Jr., H.D., Ringset, N. & Dallmann, W.K. 1989: Tertiary structures in the platform cover strata of Nordenskiöld Land, Svalbard. *Polar Research 7*, 83–93. https://doi.org/10.1111/j.1751-8369.1989.tb00359.x.

Major, H., Nagy, J., Haremo, P., Dallmann, W.K., Andersen, A. & Salvigsen, O. 1992: Geological map of Svalbard, sheet C9G Adventdalen, scale 1:100,000, preliminary edition (revised after Major and Nagy 1964), *Norsk Polarinstitutt Temakart*.

Marello, L., Ebbing, J. & Gernigon, L. 2010: Magnetic basement study in the Barents Sea from inversion and forward modelling. *Tectonophysics 493*, 153–171. https://doi.org/10.1016/j.tecto.2010.07.014.

Marshall, C., Uguna, J., Large, D.J., Meredith, W., Jochmann, M., Friis, B. & Orheim, A. 2015: Geochemistry and petrology of palaeocene coals from Spitzbergen - Part 2: Maturity variations and implications for local and regional burial models. *International Journal of Coal Geology 143*, 1–10. https://doi.org/10.1016/j.coal.2015.03.013.

Matson, R., Wolf, K. & Yancey, D. 2013: Influence of Permafrost on Seismic Imaging in Alaska. *SPE Arctic and Extreme Environments Technical Conference and Exhibition 15–17 October, Moscow, Russia*, Society of Petroleum Engineers, pp. 15–17. https://doi.org/10.2118/166821-MS.

McCann, A.J. 2000: Deformation of the Old Red Sandstone of NW Spitsbergen; links to the Ellesmerian and Caledonian orogenies. *Geological Society of London Special Publications 180*, 567–584. https://doi.org/10.1144/GSL.SP.2000.180.01.30.

McGrath, A.G. & Davison, I. 1995: Damage zone geometry around fault tips. *Journal of Structural Geology 17*, 1011–1024. https://doi.org/10.1016/0191-8141(94)00116-H.

McKerrow, W.S., Mac Niocaill, C. & Dewey, J.F. 2000: The Caledonian Orogeny redefined. *Journal of the Geological Society 157*, 1149–1154. https://doi.org/10.1144/jgs.157.6.1149.

Mège, D. & Rango, T. 2010: Permanent groundwater storage in basaltic dyke fractures and termite mound viability. *Journal of African Earth Sciences 57*, 127–142. https://doi.org/10.1016/j.jafrearsci.2009.07.014.

Merriman, R.J. 2005: Clay minerals and sedimentary basin history. *European Journal of Mineralogy 17*, 7–20. https://doi.org/10.1127/0935-1221/2005/0017-0007.

Merriman, R.J. & Peacor, D.R. 2009: Very Low-Grade Metapelites: Mineralogy, Microfabrics and Measuring Reaction Progress (chapter 2). *In* Frey, M. & Robinson, D. (eds.): *Low-Grade Metamorphism*, Blackwell Science Ltd., pp. 10–60. https://doi.org/10.1002/9781444313345.ch2.

Meyer, V., Nicol, A., Childs, C., Walsh, J.J. & Watterson, J. 2002: Progressive localisation of strain during the evolution of a normal fault population. *Journal of Structural Geology 24*, 1215–1231. https://doi.org/10.1016/S0191-8141(01)00104-3.

Midtkandal, I., Nystuen, J.P. & Nagy, J. 2007: Paralic sedimentation on an epicontinental ramp shelf during a full cycle of relative sea-level fluctuation; the Helvetiafjellet Formation in Nordenskiøld land, Spitsbergen. *Norsk Geologisk Tidsskrift 87*, 343–359.

Minakov, A., Faleide, J.I., Glebovsky, V.Y. & Mjelde, R. 2012: Structure and evolution of the northern Barents-Kara Sea continental margin from integrated analysis of potential fields, bathymetry and sparse seismic data. *Geophysical Journal International 188*, 79–102. https://doi.org/10.1111/j.1365-246X.2011.05258.x.

Miri, R., Hellevang, H., Braathen, A. & Aagaard, P. 2014: Phase relations in the Longyearbyen CO_2 Lab reservoir–forecasts for CO_2 injection and migration. *Norwegian Journal of Geology 94*, 217–232.

Morel, E.H. & Wikramaratna, R.S. 1982: Numerical modelling of groundwater flow in regional aquifers dissected by dykes. *Hydrological Sciences Journal 27*, 63–77. https://doi.org/10.1080/02626668209491086.

Mulrooney, M. & Braathen, A. 2015: Outcrop Scale Normal Faults affecting the Longyearbyen CO_2 Reservoir, Svalbard. *Poster presentation, Norsk Geologisk Forening Winter Conference, 12–14 January, Stavanger, Norway*.

Mørk, A. & Worsley, D. 2006: Triassic of Svalbard and the Barents shelf. *Boreal Triassic 3*, 23–29.

Mørk, A., Knarud, R. & Worsley, D. 1982: Depositional and diagenetic environments of the Triassic and lower Jurassic succession of Svalbard. *Arctic Geology and Geophysics 8*, 371–398.

Mørk, A., Dallmann, W.K., Dypvik, H., Johannesen, E.P., Larssen, G.B., Nagy, J. & Worsley, D. 1999: *Lithostratigraphic lexicon of Svalbard: Review and recommendations for nomenclature use: Upper Palaeozoic to Quaternary Bedrock*. Norsk Polarinstitutt, Tromsø, pp. 127–214.

Mørk, M.B.E. 2013: Diagenesis and quartz cement distribution of low-permeability Upper Triassic–Middle Jurassic reservoir sandstones, Longyearbyen CO_2 lab well site in Svalbard, Norway. *American Association of Petroleum Geologists Bulletin 97*, 577–596. https://doi.org/10.1306/10031211193.

Nagy, J. & Berge, S.H. 2008: Micropalaeontological evidence of brackish water conditions during deposition of the Knorringfjellet Formation, Late Triassic-Early Jurassic, Spitsbergen. *Polar Research 27*, 413–427. https://doi.org/10.1111/j.1751-8369.2007.00038.x.

Nejbert, K., Krajewski, K.P., Dubińska, E. & Pécskay, Z. 2011: Dolerites of Svalbard, north-west Barents Sea Shelf: age, tectonic setting and significance for geotectonic interpretation of the High-Arctic Large Igneous Province. *Polar Research* 30, 1–24. https://doi.org/10.3402/polar.v30i0.7306.

Nilsson, I., Mangerud, G. & Mørk, A. 1996: Permian stratigraphy of the Svalis Dome, south-western Barents Sea. *Norsk Geologisk Tidsskrift 76*, 127–146.

Nironen, M. 1997: The Svecofennian Orogen: a tectonic model. *Precambrian Research 86*, 21–44. https://doi.org/10.1016/S0301-9268(97)00039-9.

Ogata, K., Senger, K., Braathen, A., Tveranger, J. & Olaussen, S. 2012: The importance of natural fractures in a tight reservoir for potential CO_2 storage: a case study of the upper Triassic-middle Jurassic Kapp Toscana Group (Spitsbergen, Arctic Norway). *Geological Society of London Special Publications 374*, 395–415. https://doi.org/10.1144/SP374.9.

Ogata, K., Senger, K., Braathen, A., Tveranger, J. & Olaussen, S. 2014: Fracture systems and meso-scale structural patterns in the siliciclastic Mesozoic reservoir-caprock succession of the Longyearbyen CO_2 Lab project: implications for geologic CO_2 sequestration on Central Spitsbergen, Svalbard. *Norwegian Journal of Geology 94*, 121–154.

Ohm, S.E., Olaussen, S., Senger, K. & Johansen, I. 2017: Could uplift and erosion result in source rocks expelling huge quantities of isotopically heavy gas? Circumstantial evidence from wells on Svalbard. *The Arctic Days Conference, 29–30 May, Svolvær, Norway*, pp. 21–22.

Ohta, Y. 1982: *Hecla Hoek Rocks in Central and Western Nordaustlandet*. Skrifter 178, Norsk polarinstitutt, Oslo, 60 pp.

Osmundsen, P.T. & Andersen, T.B. 2001: The middle Devonian basins of western Norway: Sedimentary response to large-scale transtensional tectonics? *Tectonophysics 332*, 51–68. https://doi.org/10.1016/S0040-1951(00)00249-3.

Osmundsen, P.T., Andersen, T.B. & Markussen, S. 1998: Tectonics and sedimentation in the hanging wall of a major extensional detachment: the Devonian Kvamshesten Basin, western Norway. *Basin Research 10*, 213–234. https://doi.org/10.1046/j.1365-2117.1998.00064.x.

Pease, V. 2011: Eurasian orogens and Arctic tectonics: an overview (chapter 20). *Geological Society of London Memoirs 35*, 311–324. https://doi.org/10.1144/M35.20.

Petford, N. 2003: Controls on primary porosity and permeability development in igneous rocks. *Geological Society of London Special Publications 214*, 93–107. https://doi.org/10.1144/GSL.SP.2003.214.01.06.

Piepjohn, K. 2000: The Svalbardian-Ellesmerian deformation of the Old Red Sandstone and the pre-Devonian basement in NW Spitsbergen (Svalbard). *Geological Society of London Special Publications 180*, 585–601. https://doi.org/10.1144/GSL.SP.2000.180.01.31.

Pollastro, R.M. 1993: Considerations and applications of the illite/smectite geothermometer in hydrocarbon-bearing rocks of Miocene to Mississippian age. *Clays and Clay Minerals 41*, 119–133. https://doi.org/10.1346/CCMN.1993.0410202.

Polteau, S., Hendriks, B.W.H., Planke, S., Ganerød, M., Corfu, F., Faleide, J.I. & Myklebust, R. 2016: The Early Cretaceous Barents Sea Sill Complex: Distribution, $^{40}Ar/^{39}Ar$ geochronology, and implications for carbon gas formation. *Palaeogeography, Palaeoclimatology, Palaeoecology 441*, 83–95. https://doi.org/10.1016/j.palaeo.2015.07.007.

Posamentier, H.W. & Kolla, V. 2003: Seismic Geomorphology and Stratigraphy of Depositional Elements in Deep-Water Settings. *Journal of Sedimentary Research 73*, 367–388. https://doi.org/10.1306/111302730367.

Rateau, R., Schofield, N. & Smith, M. 2013: The potential role of igneous intrusions on hydrocarbon migration, west of Shetland. *Petroleum Geoscience 19*, 259–272. https://doi.org/10.1144/petgeo2012-035.

Reolid, M., Philippe, M., Nagy, J. & Abad, I. 2010: Preservation of phosphatic wood remains in marine deposits of the Brentskardhaugen Bed (Middle Jurassic) from Svalbard (Boreal Realm). *Facies 56*, 549–566. https://doi.org/10.1007/s10347-010-0219-z.

Rickard, M.J. & Belbin, L. 1980: A new continental assembly for Pangaea. *Tectonophysics 63*, 1–12. https://doi.org/10.1016/0040-1951(80)90104-3.

Riis, F., Lundschien, B.A., Høy, T., Mørk, A., & Mørk, M.B.E. (2008). Evolution of the Triassic shelf in the northern Barents Sea region. *Polar Research 27*, 318–338. https://doi.org/10.1111/j.1751-8369.2008.00086.x.

Rismyhr, B., Bjærke, T., Olaussen, S., Mulrooney, M.J. & Senger, K. in press: Facies, palynostratigraphy and sequence stratigraphy of the Wilhelmøya Subgroup (Upper Triassic–Middle Jurassic) in western central Spitsbergen, Svalbard. *Norwegian Journal of Geology 98*.

Ritzmann, O. & Faleide, J.I. 2007: Caledonian basement of the western Barents Sea. *Tectonics 26*. https://doi.org/10.1029/2006TC002059.

Rotevatn, A., Fossen, H., Hesthammer, J., Aas, T.E. & Howell, J.A. 2007: Are relay ramps conduits for fluid flow? Structural analysis of a relay ramp in Arches National Park, Utah. *Geological Society of London Special Publications 270*, 55–71. https://doi.org/10.1144/GSL.SP.2007.270.01.04.

Roy, S., Senger, K., Braathen, A., Noormets, R., Hovland, M. & Olaussen, S. 2014: Fluid migration pathways to seafloor seepage in inner isfjorden and Adventfjorden, Svalbard. *Norsk Geologisk Tidsskrift 94*, 99–199.

Sankaran, S., Rangarajan, R. & Dhar, R.L. 2005: Delineation of hydraulic connectivity across a dolerite dyke through hydrogeological, geophysical and tracer studies - A case study. *Environmental Geology 48*, 411–419. https://doi.org/10.1007/s00254-005-1230-5.

Schultz, R.A. & Fossen, H. 2008: Terminology for structural discontinuities. *American Association of Petroleum Geologists Bulletin 92*, 853–867. https://doi.org/10.1306/02200807065.

Senger, K., Tveranger, J., Planke, S., Ogata, K., Braathen, A., Wheeler, W. & Chevallier, L. 2012: Fluid flow around igneous intrusions: from outcrop to simulator. *LASI 5 Conference, 29–30 October, Port Elizabeth, South Africa*, pp. 2–3. https://doi.org/10.13140/2.1.2467.7768.

Senger, K., Roy, S., Braathen, A., Buckley, S.J., Bælum, K., Gernigon, L., Mjelde, R., Noormets, R., Ogata, K., Olaussen, S., Planke, S., Rudd, B.O. & Tveranger, J. 2013: Geometries of doleritic intrusions in central Spitsbergen, Svalbard: An integrated study of an onshore-offshore magmatic province with implications for CO_2 sequestration. *Norsk Geologisk Tidsskrift 93*, 143–166.

Senger, K., Planke, S., Polteau, S., Ogata, K., Svensen, H., Senger, K. & Svensen, H. 2014a: Sill emplacement and contact metamorphism in a siliciclastic reservoir on Svalbard, Arctic Norway. *Norsk Geologisk Tidsskrift 94*, 155–169.

Senger, K., Tveranger, J., Ogata, K., Braathen, A. & Planke, S. 2014b: Late Mesozoic magmatism in Svalbard: A review. *Earth-Science Reviews 139*, 123–144. https://doi.org/10.1016/j.earscirev.2014.09.002.

Senger, K., Tveranger, J., Braathen, A., Olaussen, S., Ogata, K. & Larsen, L. 2015a: CO_2 storage resource estimates in unconventional reservoirs: insights from a pilot-sized storage site in Svalbard, Arctic Norway. *Environmental Earth Sciences 73*, 3987–4009. https://doi.org/10.1007/s12665-014-3684-9.

Senger, K., Buckley, S.J., Chevallier, L., Fagereng, Å., Galland, O., Kurz, T.H., Ogata, K., Planke, S. & Tveranger, J. 2015b: Fracturing of doleritic intrusions and associated contact zones: Implications for fluid flow in volcanic basins. *Journal of African Earth Sciences 102*, 70–85. https://doi.org/10.1016/j.jafrearsci.2014.10.019.

Senger, K., Mulrooney, M., Braathen, A. & Ogata, K. 2016: Integrated Characterization of an Organic-rich Caprock Shale, Svalbard, Arctic Norway. *Fifth European Association of Geoscientists & Engineers Shale Workshop*. https://doi.org/10.3997/2214-4609.201600430.

Senger, K., Millett, J., Planke, S., Ogata, K., Eide, C.H., Festøy, M., Galland, O. & Jerram, D.A. 2017: Effects of igneous intrusions on the petroleum system: a review. *First Break 35*, 1–10.

Singhal, B.B.S. & Gupta, R.P. 2010: Fractures and Discontinuities. In *Applied Hydrogeology of Fractured Rocks*. Springer Science & Business Media, pp. 13–33. https://doi.org/10.1007/978-90-481-8799-7.

Smelror, M., Petrov, O., Larsen, G.B. & Werner, S. 2009: *Geological History of the Barents Sea*. Geological Survey of Norway, Trondheim, Norway, pp. 44–52.

Smit, P.J. 1978: Groundwater recharge in the dolomite of the Ghaap Plateau near Kuruman in the Northern Cape, Republic of South Africa. *Water SA 4*, 81–92.

Souche, A., Beyssac, O. & Andersen, T.B. 2012: Thermal structure of supra-detachment basins: a case study of the Devonian basins of western Norway. *Journal of the Geological Society 169*, 427–434. https://doi.org/10.1144/0016-76492011-155.

Sruoga, P., Rubinstein, N. & Hinterwimmer, G. 2004: Porosity and permeability in volcanic rocks: A case study on the Serie Tobifera, South Patagonia, Argentina. *Journal of Volcanology and Geothermal Research 132*, 31–43. https://doi.org/10.1016/S0377-0273(03)00419-0.

Stearns, H.T. 1942: Hydrology of volcanic terranes. *In* Meinzer, O.E. (ed.): *Hydrology*, Dover Publishing Inc., New York, pp. 678–703.

Steel, R.J. & Worsley, D. 1984: Svalbard's post-Caledonian strata - an atlas of sedimentational patterns and palaeogeographic evolution. *In* Spencer, A.M. (ed.): *Petroleum Geology of North European Margin*, Springer Netherlands, pp. 109–135. https://doi.org/10.1007/978-94-009-5626-1_9.

Steel, R., Gjelberg, J., Helland-Hansen, W., Kleinspehn, K., Nottvedt, A. & Rye-Larsen, M. 1985: The Tertiary strike-slip basins and orogenic belt of Spitsbergen. *In* Biddle, K.T. & Christie-Blick, N. (eds.): *Strike-Slip Deformation, Basin Formation, and Sedimentation*, SEPM Society for Sedimentary Geology 37, pp. 339–359. https://doi.org/10.2110/pec.85.37.0339.

Stemmerik, L. & Håkansson, E. 1989: Stratigraphy and depositional history of the Upper Palaeozoic and Triassic sediments in the Wandel Sea Basin, central and eastern North Greenland. *Rapport Grønlands Geologiske Undersøgelse GGU-R-143*, pp. 21–45.

Stemmerik, L. & Worsley, D. 1989: Late Palaeozoic sequence correlations, North Greenland, Svalbard and the Barents Shelf. *In* Collinson, J.D. (ed.): *Correlation in hydrocarbon exploration*, Springer Netherlands, pp. 99–111. https://doi.org/10.1007/978-94-009-1149-9_10.

Talwani, M. & Eldholm, O. 1977: Evolution of the Norwegian-Greenland Sea. *Geological Society of America Bulletin 88*, 969–999. https://doi.org/10.1130/0016-7606(1977)88<969:EOTNS>2.0.CO;2.

Tharp, T.M. 1987: Conditions for Crack-Propagation by Frost Wedging. *Geological Society of America Bulletin 99*, 94–102. https://doi.org/10.1130/0016-7606(1987)99<94:cfcpbf>2.0.co;2.

Thomaz Filho, A., Mizusaki, A.M.P. & Antonioli, L. 2008: Magmatismo nas bacias sedimentares brasileiras e sua influência na geologia do petróleo. *Revista Brasileira de Geociências 38*, 128–137. https://doi.org/10.25249/0375-7536.2008382S128137.

Throndsen, T. 1982: Vitrinite Reflectance Studies of Coals and Dispersed Organic Matter in Tertiary Deposits in the Adventdalen Area, Svalbard. *Polar Research 1982*, 77–91. https://doi.org/10.1111/j.1751-8369.1982.tb00478.x.

UNIS CO_2 Lab AS 2015: Longyearbyen CO_2 lab - Phase II Final Report, http://co2-ccs.unis.no/Pdf/Longyearbyen%20CO2%20lab%20Phase%202%20Report_10_2015.pdf.

Van Stappen, J., de Kock, T., Boone, M.A., Olaussen, S. & Cnudde, V. 2014: Pore-scale characterisation and modelling of CO_2 flow in tight sandstones using X-ray micro-CT; Knorringfjellet Formation of the Longyearbyen CO2 lab, Svalbard. *Norsk Geologisk Tidsskrift 94*, 201–215.

Van Stappen, J.F., Meftah, R., Boone, M.A., Bultreys, T., de Kock, T., Blykers, B.K., Senger, K., Olaussen, S. & Cnudde, V. 2018: In Situ Triaxial Testing To Determine Fracture Permeability and Aperture Distribution for CO_2 Sequestration in Svalbard, Norway. *Environmental Science & Technology 52*, 4546–4554. https://doi.org/10.1021/acs.est.8b00861.

Van Wyk, W.L. 1963: *Ground-water studies in northern Natal, Zululand and surrounding areas*. Geological Survey of South Africa Memoir 52, Republic of South Africa, Pretoria, 145 pp.

Vasco, D.W., Ferretti, A. & Novali, F. 2008: Reservoir monitoring and characterization using satellite geodetic data: Interferometric synthetic aperture radar observations from the Krechba field, Algeria. *Geophysics 73*, WA113. https://doi.org/10.1190/1.2981184.

Walsh, J.J. & Watterson, J. 1991: Geometric and kinematic coherence and scale effects in normal fault systems. *Geological Society of London Special Publications 56*, 193–203. https://doi.org/10.1144/GSL.SP.1991.056.01.13.

Wangen, M., Souche, A. & Johansen, H. 2016: A model for underpressure development in a glacial valley, an example from Adventdalen, Svalbard. *Basin Research 28*, 752–769. https://doi.org/10.1111/bre.12130.

White, D.J., Burrowes, G., Davis, T., Hajnal, Z., Hirsche, K., Hutcheon, I. & Whittaker, S. 2004: Greenhouse gas sequestration in abandoned oil reservoirs: The International Energy Agency Weyburn pilot project. *Geological Society of America Today 14*, 4–11. https://doi.org/10.1130/1052-5173(2004)014<004:GGSIAO>2.0.CO;2.

Whittaker, S., White, D., Law, D. & Chalaturnyk, R. 2004: IEA GHG Weyburn CO2 Monitoring & Storage Project Summary Report 2000-2004. *From the proceedings of the 7th International Conference on Greenhouse Gas Control Technologies held, 5–9 September, Vancouver, Canada*, p. 283.

Wierbowski, A., Kulicki, C. & Pugaczewska, H. 1981: Fauna and stratigraphy of the uppermost Triassic and the Toarcian and Aalenian deposits in the Sassenfjorden, Spitzbergen. *Acta Palaeontologica Polonica 26*, 196–240.

Worsley, D. 1973: The Wilhelmøya Formation–a new lithostratigraphical unit from the Mesozoic of eastern Svalbard. *Årbok Norsk Polarinstitutt*, 7–16.

Worsley, D. 2008: The post-Caledonian development of Svalbard and the western Barents Sea. *Polar Research 27*, 298–317. https://doi.org/10.1111/j.1751-8369.2008.00085.x.

Xue, Z., Tanase, D. & Watanabe, J. 2006: Estimation of CO_2 saturation from time-lapse CO_2 well logging in an onshore aquifer, Nagaoka, Japan. *Exploration Geophysics 37*, 19–29. https://doi.org/10.1071/EG06019.

Ziegler, P.A. 1988: Post-Hercynian plate reorganization in the Tethys and Arctic-North Atlantic domains (chapter 30). *Developments in Geotectonics 22*, 711–755. https://doi.org/10.1016/B978-0-444-42903-2.50035-X.

Appendix 1

Core samples from boreholes and outcrops were collected for pore network characterisation, and analysed using high-resolution X-ray computed tomography (micro-CT; Cnudde & Boone, 2013; Van Stappen et al., 2014). This method allowed spatial resolutions down to 2.8 μm to be achieved. To ensure maximum resolution, subsamples were taken from original core samples, thereby limiting the analysed volume. Image reconstruction and analysis was carried out using the Octopus software suite (Brabant et al., 2011). The analysis focused on the 3D pore structure and the presence of micro-cracks (Van Stappen et al., 2014). However, due to the systematic limitations related to the focal spot size of the X-ray source, the pore space is often not fully represented even in scans with the highest achievable resolution (on the order of 1 μm). This is especially true in very tight sandstones, as in the Wilhelmøya Subgroup, where pores smaller than the resolution limits are present. In order to fully characterise the pore network, micro-CT was combined with other techniques, notably Mercury Intrusion Porosimetry (MIP; Cnudde et al., 2009) and Helium porosimetry (HeP; Van Stappen et al., 2014).

In an initial campaign, 24 sandstone core samples (3 from DH2, 9 from DH4 and 12 from outcrop) were chosen for micro-CT analysis, using a Feinfocus X-ray source and a Varian 2520 V Paxscan panel detector. In combination with He-porosimetry and MIP, the full pore space was evaluated (Van Stappen et al., 2014). Furthermore, micro-CT investigations allowed the quantitative analysis of fracture orientation, length and maximum aperture. In this case, fracture length is calculated as the diameter of the circumscribed sphere around a 3D object, while the maximum fracture aperture is defined as the maximum inscribed sphere fitting in this 3D object (Brabant et al., 2011).

In order to determine fracture apertures in CT images, the fracture is segmented from the overall rock matrix. Next, the fracture is virtually packed with spheres having their central points in the middle of the fracture. Finally, the diameters of these spheres are increased until they reach the fracture walls. As a consequence, the accuracy of fracture aperture measurements is limited to integral multiples of the image resolution. Nonetheless, this method adequately describes fracture aperture distribution.

Appendix 2

Clay gouge from 5 normal faults affecting the reservoir were sampled from outcrops in Konusdalen (Fig. 2) and subject to X-Ray diffraction (XRD) mineralogical composition analyses. A background sample from a shale-rich bed within the Wilhelmøya Subgroup and outside of the fault damage zones was also analysed. Samples were initially treated in bulk to derive cumulative XRD mineralogical composition. Rietveld refinement was then applied, i.e., a technique where the neutron and X-ray diffraction of powder samples results in a pattern characterised by reflections (peaks in intensity) at certain positions. This process was challenging, possibly due to structural complexity. Even though microstrain corrections were applied, it was not possible to remove the effect completely. The second part of the analysis attempted to model clay fraction aggregates. Samples were washed using Milli-Q water, i.e., ultrapure water (Type 1), before clay fraction separation. Sodium bicarbonate was added to the suspension to obtain better dispersion. The grain size fraction (<2 μm) was extracted based on the principles of Stokes' law and placed on a circular glass sample holder using the Millipore filter transfer method. The uppermost part of the suspended material (clay fraction) was removed or extracted using a siphon. Analysis was run using a D8 advanced Bruker diffractometer equipped with Copper Ka radiation (40 kV and 40 mA) and LynxEye detector. The data were collected from 2 to 65 degrees 2q for air-dried samples and 2–35 degree 2q for ethylene glycol and heat-treated samples. Each sample was subject to four methods of analysis: 1) air drying, 2) Ethylene glycol solvation carried out in a desiccator at 60°C over 12 hours. 3) heating to 350°C and 550°C for an hour to ensure proper identification of mixed-layer clays, and to differentiate between chlorite and kaolinite, respectively. Clay phases in each sample follow the USGS clay mineral identification flow diagram. NEWMODE II was used to quantify the clay fractions, and input data were adjusted until a satisfactory fit of peak positions, shapes and intensities in the entire XRD profile was reached compared to theoretical patterns. This modelling gives a good estimate of the relative abundance of each clay mineral with respect to each sample.